ISRN LUTMDN/TMHP—10/5228—SE
ISSN 0282-1990

Product losses of Highly Viscous Products in Pipe Systems during Displacement Processes

Johan Abrahamsson

Thesis for the Degree of Master of Science

Division of Fluid Mechanics
Department of Energy Sciences
Faculty of Engineering
Lund University

Abstract

It is common in the process industry to displace one fluid by another. During the displacement process an unwanted mixing between the two phases is unavoidable and being able to estimate this mixing is of great importance when trying to minimize product losses and improving the quality of the final product.

A method for simulating the displacement process using commercial CFD codes was developed and the effect from varying the fluid parameters was simulated. The method was verified by comparing the results to experimental data. The method was accurate at estimating the breakthrough time but failed to predict the outflow of the residual film.

Finally a simple method based on the maximum velocity of the displaced fluid was investigated delivering accurate predictions of the breakthrough time.

Acknowledgements

The thesis was carried out for Tetra Pak.

I would like to thank supervisors Johan Revstedt at the Division of Fluid Mechanics at Lund University and Fredrik Innings at Tetra Pak Processing Systems. I would also like to thank Michael Olsson and the people at Tetra Pak flow group for their assistance during the project.

Lund, February 2011

Johan Abrahamsson

Contents

Notations

Latin

D	Diffusion (m^2/s)
d_d	Particle diameter of dispersed phase (m)
f	Friction factor (-)
g	Gravity (m/s^2)
k	Turbulent kinetic energy (m^2/s^2)
K	Consistency index (Pas^n)
n	Flow behaviour index (-)
p	Pressure (Pa)
r	Current radius (m)
Q	Volumetric flow rate (m^3/s)
R	Total radius (m)
L_s	Characteristic length scale of the system (m)
V_s	Characteristic velocity of the fluid (m/s)
V_{max}	Maximum velocity (m/s)
t_D	Displacement time (s)
t_P	Displacement time for plug (s)
U	Velocity (m/s)
$\overline{U}$	Averaged velocity (m/s)
$\overline{U}_{max}$	Mean maximum velocity (m/s)
u’	Fluctuating velocity (m/s)
u_t	Friction velocity (m/s)
y^+	Dimensionless wall distance (m)

Greek

α	Volume fraction (-)
γ	Shear rate (1/s)
ρ	Density (kg/m^3)
ε	Dissipation (m^2/s^3)
η_D	Displacement efficiency (-)
η_r	Relative viscosity (-)
κ	Viscosity ratio (-)
μ	Dynamic viscosity (Pas)
τ	Shear stress (Pa)
τ_w	Wall shear stress (Pa)
τ_0	Critical shear stress (Pa)
τ^*	Cross law critical shear stress (Pa)
ν	Kinematic viscosity ($Pasm^3/kg$)
ν_t	Turbulent kinematic viscosity ($Pasm^3/kg$)
φ	Volume fraction (-)

Dimensionless numbers

Re	Reynolds number
Sc_t	Turbulent Schmidt number
St	Stokes number

1. Introduction

The behaviour of the displacement process of one fluid by another in pipes is an important case in many industrial applications. Industries where this process commonly is of importance are the food and the oil industry. In the food industry the process is important when changing products in the machines and during cleaning of the system. Often the rheologies of the encountered fluids are non-Newtonian and fluid characteristics such as slip and yield stress may have a large impact on the displacement.

During the displacement process a front of the displacing fluid will penetrate the displaced fluid in the shape of a finger with a higher velocity than the surrounding displaced fluid. This will result in the displacing fluid reaching the outlet before the displaced and the displacement is considered to be inefficient. The front of the displacement process for two cases is shown in figure 1.

The most important parameter for the fluid displacements is the breakthrough time which is the time it takes for the displacing fluid to reach the outlet. At this point, if the flow is not redirected into a waste tank the product will end up diluted which is only acceptable in very limited quantities. Other characteristics of the displacement process such as the thickness of the wall film and the time it takes to completely clean the pipe system are usually less important.

Knowledge about how the displacement process works and accurately being able to estimate it correctly is very useful since a choice must be made as of when to redirect the flow into a waste tank. An accurate estimation of the displacement process is essential for minimizing product losses and to make sure that no or very little water will end up in the final product. Other uses of this knowledge are when designing the machines and for estimating the costs of various operations which is of interest for the companies using the machines.

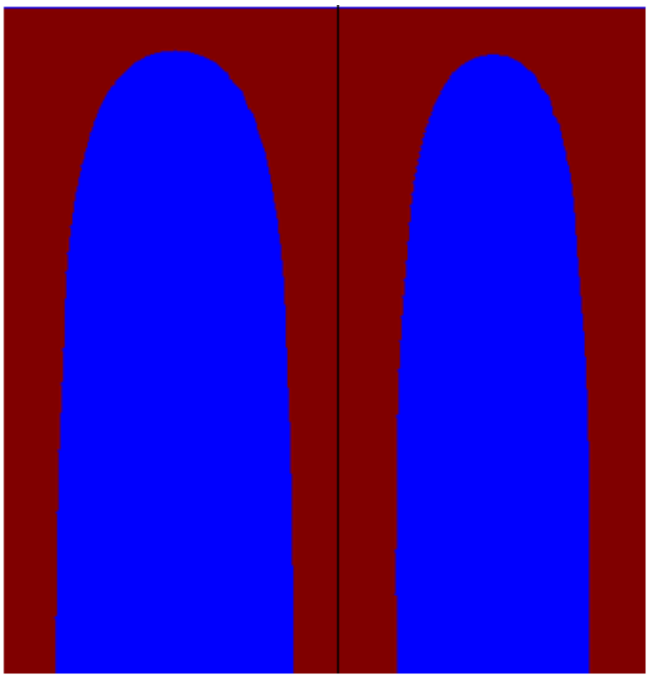

Figure 1 Displacement of a Newtonian fluid (left) and a shear thinning fluid (right)

1.2 Objectives

The objective of this master thesis is to find a method for estimating the displacement process of one product by another in pipes for Tetra Pak. The method shall be based on Computational Fluid Dynamics (CFD) using the commercial software Fluent from ANSYS.

The results shall be verified with experimental data from the displacement process obtained from Tetra Pak.

Also sensitivity studies to rheological data shall be made and important fluid properties for the displacement examined.

The accuracy of a simple model for estimating the displacement process based on the maximum velocity of the displaced fluid is also discussed.

2. Previous work and background

The displacement of one product by another is frequently encountered in the machines and in the pipes connecting the machines to the storage tanks each time the products are changed and during washing of the system. Every time a product is being displaced in a machine or while being transported to the machine from the storage tank, a large zone consisting of both fluids will be created with water in the centre being surrounded by an annulus of the product as can be seen in figure 1. Because most of the product in this two phase zone will be considered to dilute to sell, the displacement process is very wasteful and large savings can be made by reducing this two phase zone. Another problem is the residuals of the displaced fluid covering the walls and it is important to be able to estimate how fast it will wash away so as to avoid unwanted mixing when filling the machine with a new product and to minimize the use of washer fluids which can be expensive in large volumes.

During the displacement process the displacing fluid will penetrate the displaced fluid and a residual fluid film of the displaced fluid will be left along the walls. The thickness of the residual fluid film is largely determined by the viscosity and density ratios of the two fluids.

The existence of yield stress in the fluid and wall slip will also have an impact on the residual film and the displacement process. This wall film will continuously decrease in thickness as it is initially a flat fluid-fluid interface and its shape is later created by a velocity profile. Further wall film decreasing effects are caused by instabilities present in the flow and mass transfer between the fluids which removes displaced fluid from the residual film and into the faster flowing displacing fluid [1].

When discussing the displacement process it is common to measure the displacement efficiency. The displacement efficiency η_D is defined as the ratio between the time it takes the displacement front to reach the outlet t_D divided by the time it would take for a perfect plug t_P.

$$\eta_D = \frac{t_D}{t_P}$$

Eq. 1-1

The time it takes for the displacing fluid to reach the outlet t_D is commonly referred to as the breakthrough time and is the most important parameter to accurately be able to determine.

Investigations of the displacement process are usually based on one of two different methods. Either the flow rate of the various fluid are being measured or the area ratio between the two fluids. Because the velocity profiles for the two different fluids are determined by the rheology and density of the two fluids, there is no strict connection between the outflow ratio of the two fluids and the phase distribution or residual film thickness in the pipe. This is exemplified in figure 2 where the phase distribution in the pipe is equal but the velocity profiles and thus the outflow ratios are different.

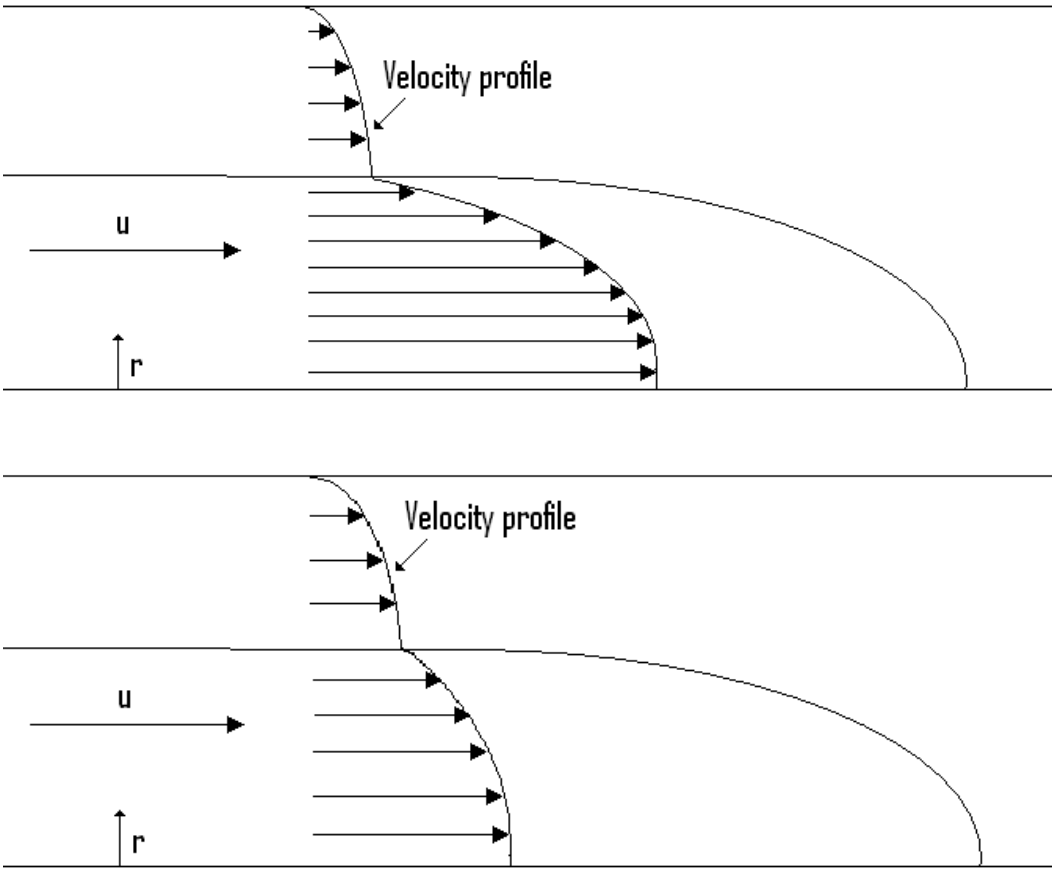

Figure 2 Velocity profiles for two cases with identical phase distribution but different viscosity ratio

A large number of experiments on the displacement process of a laminar fluid by another laminar fluid have been published. One of the first series of published experiments on the displacement process was conducted by Tailor in 1953 [2].

A comprehensive series of experiments measuring the residual film of various Newtonian, shear thinning and yield stress fluids in laminar-laminar displacement processes in pipes for a wide range of velocities are reported by Gabard et al. [1]. The displacement of miscible and immiscible fluids in vertical and horizontal capillary tubes has also been experimentally investigated [3, 4, 5]. The case of vertical and horizontal low velocity displacement in Hele-Shaw cells which is displacement between two planes has also been experimentally investigated [3, 4]. Numerical studies of the viscous fingering behaviour of non Newtonian fluids in horizontal Hele-Shaw cells have also been examined [6]. The special case of displacement in annular pipes of a low viscosity fluid by a more viscous fluid which is a common situation in oil drilling operations has been verified as very efficient by experiments [7].

Newtonian fluids

When displacing Newtonian fluids, the residual film thickness increased with increasing velocity until a high-velocity limit is reached and no further effect from velocity can be measured [1]. Numerical simulations and experiments show a growing initial residual film

thickness with increased viscosity ratio[1, 3]. Similar to the effect from increasing the velocity, an upper viscosity ratio limit was reached both experimentally and from numerical simulations above which no further growth of the initial residual film was detected [1,3].

Experimental results propose the existence of a minimum finger thickness limit for the displacing fluid in the Newtonian case [6]. Numerical simulations of Hele-Shaw cells case also indicate on the existence of a threshold viscosity ratio below which the displacement front is moved by the velocity field in the case of minimal diffusion [8]. The experiments of displacement of a Newtonian fluid in horizontal pipes indicated the development of a downward dimple in the displacing fluid as shown in figure 3 [4]. Stokes flow simulations of the gravitational effect on the displacement efficiency in horizontal pipes showed a slight reduction in displacement efficiency with decreased density difference between the fluids [12]. Similar simulation of the effect of diffusion also resulted in an increased displacement efficiency with increased diffusion [12].

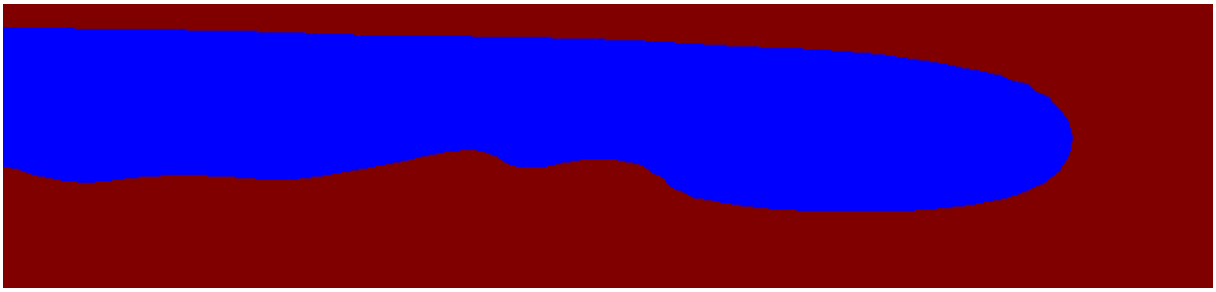

Figure 3 Horizontal displacement of fluids with different density

During the experiments of displacement of Newtonian fluids in horizontal capillary tubes which could be up to 4 mm in diameter, a finger splitting behaviour was seen. This means that the displacement finger split in two which is thought to be created by gravity induced streams in the flow [4].

Shear thinning fluids

When displacing shear thinning liquids, the residual film thickness unlike Newtonian decreases with increasing velocity until it similar to Newtonian fluids reached a minimum value where it stabilized. The residual thickness displayed strong coupling to the shear thinning coefficient and decreased with increasing shear thinning characteristics [1]. No minimum width of the displacement front exists for shear thinning fluids which can be very thin [6]. For a comparison of the displacement front of a Newtonian and a shear thinning fluid see figure 1. Experiments on decreasing the velocity of shear thinning fluids resulted in the residual film thickness approaching the values of displacing a Newtonian fluid. This was likely due to the shear thinning fluid approaching a Newtonian behaviour at low shear rates [1].

Yield stress fluids

Experiments on yield stress fluids showed a considerable effect from the yield stress which had a decreasing effect on the initial residual film thickness. When displacing yield stress fluids, the residual film thickness increases with an increase in velocity unlike for shear

thinning fluids which decreased. This effect of velocity changes for various fluids is summarized in table 1. The initial residual film thickness gets thinner with a larger yield stress [1]. Another difference is the possible case of a static residual film which has no instabilities and thus keeps its thickness as the displacing fluid passes in the immiscible case. This can be seen for the case of a Newtonian fluid displacing a yield stress fluid in figure 4.

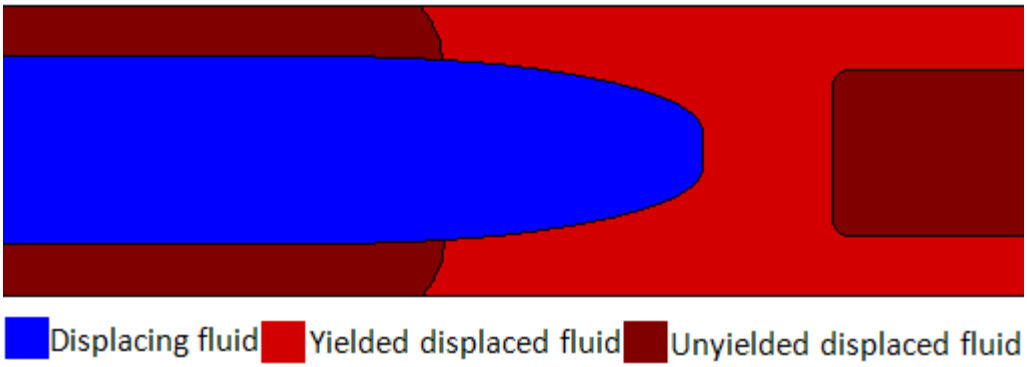

Figure 4 Yield stress fluid displacing yield stress fluid

Numerical stokes flow simulations of creeping displacement of a yield stress fluid demonstrate that a recirculation zone is formed in the gap in front of the displacing fluid and the unyielded zone in the displaced fluid. Successful attempts at predicting the residual film thickness based on the thickness of the recirculation zone has been made [9]. This implies that the flow in the region in front of the displacement front has a big influence on the displacement process.

Gabard's experiments [1] on the displacement of yield stress fluids indicated 3 different displacement cases. For high enough yield stress the fluid was displaced as a plug pushed in front of the displacing fluid. At lower yield stress the displacing fluid penetrated the yield stress fluid and the displacement process was similar to the displacement of a shear thinning fluid but with a flat displacement front. A third case was also seen which was described by Gabard et al [1]. as the fracturing of a solid and the displaced fluid did not leave the solid state during the displacement.

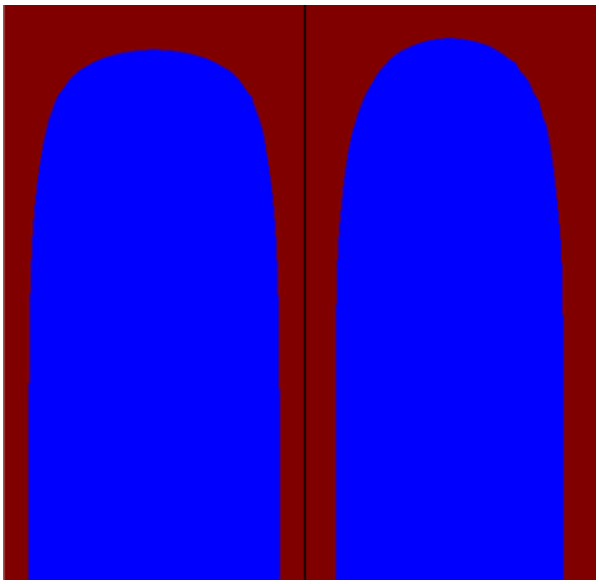

Figure 5 Displacement of a yield stress fluid at low velocity to the left and high velocity to the right

Another similar behaviour of the displacement of yield stress fluids is footprinting which happens when the yield stress fluids wall film becomes static and any variation of the film present during the solidification will be preserved causing the water to flow around [9].

Gabard et al. also simulated axisymmetric displacement processes using finite volume method and verified the results with experimental results. The comparison showed a good agreement except for low velocity simulations and displacement processes with very high or low viscosity ratio [1].

Fluid being displaced	Newtonian	Shear thinning	Yield stress fluid
Effect on residual film thickness from increased velocity	Increasing	Decreasing	Increasing

Table 1: Effect on the residual film thickness with velocity variation

Analytical and numerical methods

Only a few analytical models describing the displacement process has been published [10], [11]. A more common method for estimating the process is numerical methods. The most commonly published method is stokes flow simulations which are only valid for creeping flow at Re<<1 [3, 5, 12, 13]. Another commonly used method is the volume of fluid method which unlike stokes flow simulations are valid at for Re>1 [1, 3, 14, 15]. Other attempted methods are Asymptotic transverse flow equilibrium (TFE) simulations, BGK lattice gas technique and Arbitrary-Lagrange-Euler (ALE) simulations [16, 22, 8]. The Marker and cell method has been used to investigate instabilities of low Reynolds number flow in vertical pipes [17]. Numerical studies of the case where the immiscible fluids are fully mixed in pipe flow have been simulated using the Eulerian-Eulerian method [18].

2.2 Instabilities

During the displacement of a fluid by another the process is complicated by the multiple instabilities that might arise. These instabilities can be organized into three groups depending on the different scales of the displacement process they describe.

Instability	Cause
Rayleigh Taylor	Density difference between fluids during displacement
Saffman Taylor	Viscosity difference between fluids during displacement
Axisymmetric	Large scale displacement pattern
Corkscrew	Large scale displacement pattern
Pearly	Large scale displacement pattern
Kelvin Helmholz	Velocity shearing
Yih	Viscosity stratification
Plateau–Rayleigh	Surface tension

The most fundamental group of instabilities is the entire displacement process and the question of whether the displacing fluid will penetrate the displaced fluid or simply push it forward. In a vertical pipe with the heavier fluid on top of the lighter a Rayleigh-Taylor instability will arise while the opposite situation is stable.

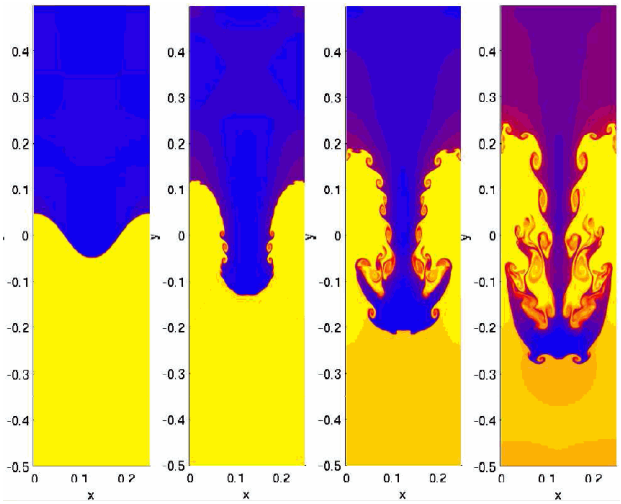

Figure 6 Numerical simulation of Rayleigh Taylor instability which is the large instability. Kelvin-Helmholz instabilities are developing on the side of the Rayleigh Taylor instability [23]

Similarly a more viscous fluid displacing a less viscous fluid is unstable for the Saffman-Taylor instability.

Structures and geometry

Another group of instabilities are the large scale fingering instabilities experienced during the displacement process. These instabilities describe the shape and path of the displacement finger. These are experimentally studied rather than mathematically derived from differential equations like Orr-Somerfeld. These large scale instability patterns such as axisymmetric and corkscrew instabilities have been investigated for low velocity flow in vertical capillary tubes [19]. The various instabilities can be seen in figure 7.

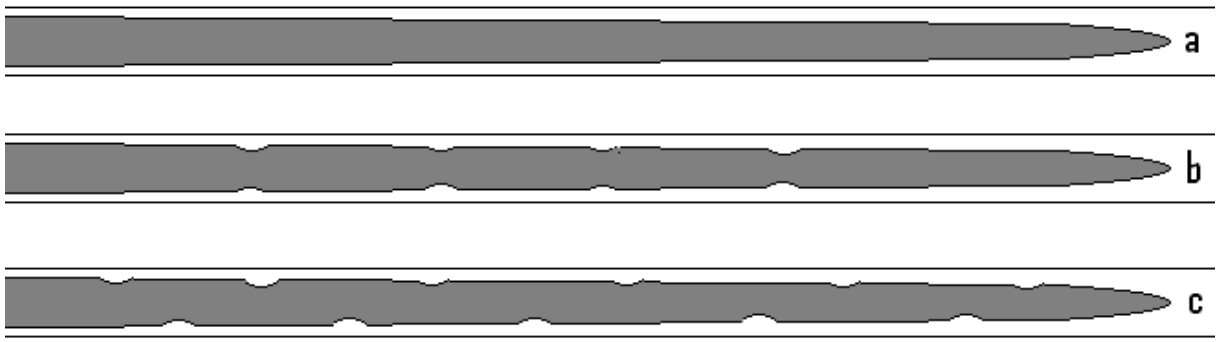

Figure 7 (a) stable displacement (b) axisymmetric instability (c) Corkscrew instability

Investigations of these kinds of instabilities for vertical displacement show an increasing stability with viscosity ratio and density difference and a decrease in stability with increasing velocity [19]. Another kind of instability is the complete disintegration of the jet into droplets which arises under certain circumstances. A similar instability caused by surface tension is the Plateau-Rayleigh instability which can be seen when water drops form from a tap.

The third group of instabilities describe the instabilities formed at the interface between two fluids of different viscosity, velocity and density. Some of the first and most frequently referenced analysis's of instabilities between two layers of fluids were made by Yih who showed that the flow of two equally dense fluids in layers with a variation in viscosity unlike single fluid flow could be unstable for all Reynolds numbers. The existence of these Yih instabilities which were caused by viscosity stratification was determined by Reynolds number, viscosity ratio and film layer thickness [24].

Further studies of pipe flow have showed that the viscosity stratification for a less viscous fluid displacing a more viscous fluid is always unstable while the opposite process is unstable only for certain film thickness ratios, viscosity ratios and Reynolds numbers [25].

Another instability experienced during the displacement process is the Kelvin-Helmholtz instability which originates from the different velocities of the two fluids. The instability is stabilized by surface tension and a density ratio when the denser fluid is beneath a lighter. In the case of zero surface tension the scenario is always unstable for all velocity and density

ratios for a short enough wavelength. The case of two equally dense fluids without surface tension is Kelvin Helmholz unstable for all wavelengths [26].

Experiments of the displacement of yield stress fluids indicate that such displacement is always stable as no instabilities were present in the interval of displacement velocities investigated [1]. This is expected since the fluid film will be static for displacement velocities below a threshold value. The front of a displacement process for various velocities as shown in figure 5.

Theoretical investigation concerning under what conditions the residual film is static for yield stress fluids has been made by Allouche et al.[3]. The instability patterns when displacing a yield stress fluid in Hele-Shaw cells has specifically been investigated by Zorin et al.[8].

All published experimental investigations of instabilities are made at very low velocities and few results are described in other ways than as a description of the behaviour experienced. Little is thus known about what instabilities is to be expected during the turbulent-laminar displacements in pipes that are being simulated in this thesis. The determination of existence of instabilities is further complicated by the displacement of non-Newtonian fluids with poorly known behaviour.

The phase distribution of yoghurt in a pipe after 5 meters of flow with an inlet velocity of 1 m/s plotted against time can be seen in figure 8 [19]. Measurements were made by ERT with a frequency of 6 Hz and optimized for temporal accuracy. A highly mixed state can be seen indicating high mass transfer or instabilities.

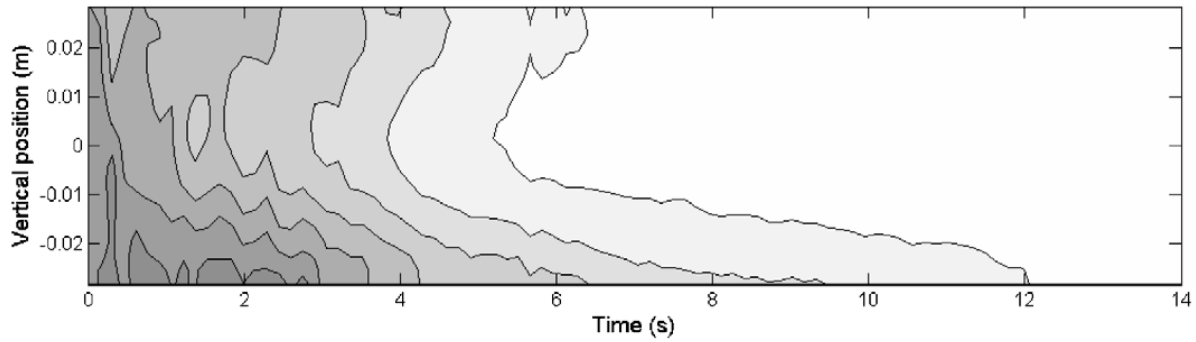

Figure 8 ERT simulation of yoghurt [19]

3. Theory

3.1 Governing equations

The behaviour of fluid flow can be summed up into a group of partial differential equations. For viscous and incompressible fluids with no heat transfer there are 4 governing equations, the continuity, the momentum and the mass fraction equation.

The first of the governing equations is the continuity equation which is derived from the law of conservation of mass which states that no mass can be created nor destroyed. Thus, the change of mass inside a control volume must equal the difference between the mass transported in and out of the control volume. For an incompressible fluid this change must be zero.

$$\frac{\partial u_i}{\partial x_i} = 0$$

Eq. 3-1

The second, third and fourth of the governing equations are the laws of conservation of momentum in three dimensions. They are derived from Newton's second law of motion which states that the acceleration multiplied with the mass of an element must equal the forces applied on the element.

There are two kinds of forces acting on a fluid element, body and surface forces. In displacement processes the only important body force is gravity and the most important surface forces are pressure, viscous and surface tension forces.

$$\rho \frac{\partial u_i}{\partial t} + \rho u_j \frac{\partial u_i}{\partial x_j} = \rho g_i - \frac{\partial p}{\partial x_i} + \mu(\frac{\partial^2 u_i}{\partial x_j \partial x_j})$$

Eq. 3-2

These four equations are commonly referred to as the Navier Stokes equations which also include a conservation of energy equation which has been omitted here because there is no heat transfer present. When deriving the Navier-Stokes equation an assumption of the fluids having a Newtonian behaviour has been made. For Newtonian fluids there is a constant relation between the shearing and the applied shear stress of a fluid. It is assumed that the non Newtonian behaviour can be approximated by an apparent viscosity for each applied shear rate and that the equations are still valid.

Various extra equations for handling the multiphase flow are also solved but are method dependent and are described in section 3.5.

3.2 Rheology

Rheology is the study of fluid viscosity. Incompressible fluids can be divided into two main groups Newtonian and non-Newtonian. Newtonian fluids are defined as fluids with a linear and time independent relationship between shear rate and shear stress. The ratio of these two is defined as the fluids viscosity. For non-Newtonian fluids however the ratio is not linear and may be time dependent.

Non Newtonian fluids can further be divided into subgroups by many different categories such as shear thinning and shear thickening fluids. Shear thinning fluids show a decreasing apparent viscosity with increasing shear stress while the apparent viscosity increases for shear thickening. Typical shear thinning fluids are polymers and dairy products while typical shear thickening fluids are starch solutions and some granular suspensions.

Other ways to categorize non-Newtonian fluids are by time dependence on the viscosity. Thixotropic fluids have a decreasing apparent viscosity with time and the less common rheopectic fluids have an increasing apparent viscosity with time. Thixotropic behaviour is usually caused by a breakdown of the microstructure of the fluid.

Another important characteristic of many non-Newtonian fluids is yield stress. Yield stress or pseudo plastic fluids behave as a solid when exposed to a shear stress below a threshold value above which the solid changes characteristics to a fluid. When modelling yield stress fluids in Fluent, the unyielded zone is treated like a highly viscous fluid.

Most high viscosity dairy products exhibit non-Newtonian fluid characteristics which creates multiple problems when modelling their flow using CFD. Unlike Newtonian fluids, it is complicated to achieve accurate estimations of the viscosity parameters for non-Newtonian fluids since they are shear stress and history dependent. Fluid behaviour, such as yield stress and slip further complicate the estimation of rheological parameters. Thus only a rather low accuracy from measurements can be expected.

The simulation of non-Newtonian fluids is further complicated by the little amount of knowledge about their turbulent and near turbulent behaviour.

When calculating the flow of non-Newtonian fluids the viscosity needs to be estimated by an algebraic model and the parameters of the model needs to be curve fitted to experimental data.

Fluent offers 3 models for calculating the viscosity of temperature independent non-Newtonian fluids:

Power law

The power law is the most commonly used non-Newtonian viscosity model and it is the one that most accurately describes the behaviour of most dairy products with the exclusion of yield stress fluids. The viscosity of a power law fluid is described by a consistency index and a flow behaviour index and the shear rate $\dot{\gamma} = \frac{\partial u}{\partial y}$ in a nonlinear function: $\mu = K * (\dot{\gamma})^{n-1}$

The behaviour index n describes weather the fluid is shear thinning n<1, Newtonian n=1 or dilatant n>1.

The velocity profile of fully developed laminar pipe flow of a power law fluid is described by [27]:

$$V = V_{mean} * \left(\frac{3 * n + 1}{n + 1}\right) * \left(1 - (\frac{r}{R})^{\frac{n+1}{n}}\right)$$

Eq. 3-3

The profiles are plotted for various behaviour indexes in figure 11.

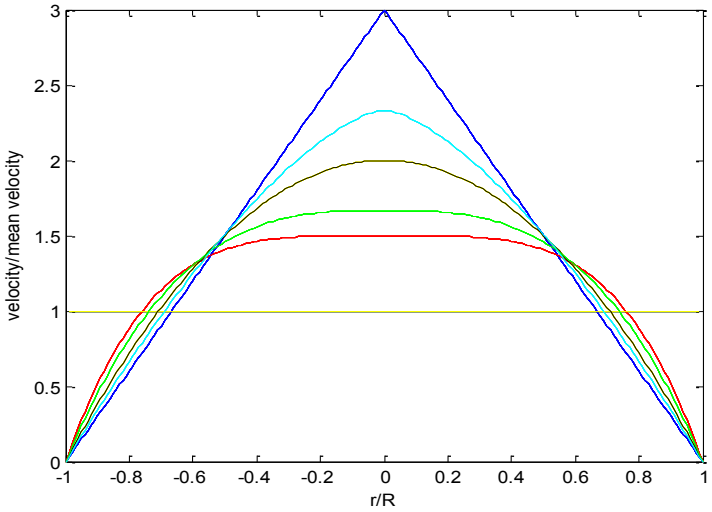

Figure 11 Power law velocity profiles, black n=1, cyan n=2, blue n=1000, green n=0.5, red n=0.333, yellow n=0

The maximum velocity for power law fluids can be calculated from :

$$V_{max} = V_{mean} * \left(\frac{3 * n + 1}{n + 1}\right)$$

Eq. 3-4

Cross

The cross model is similar to the Power law for high shear rate flow and approaches Newtonian with viscosity μ_0 during low shearing of the flow with shear rate less than τ^*:

$$\mu = \frac{\mu_0}{1 + \lambda\dot{\gamma}^{1-n}}$$

Eq. 3-5

Where p is the power law index and $\lambda=\frac{\mu_0}{\tau^*}$ is the inverse of the shear rate at which the fluid changes behaviour from Newtonian to power law. Note that the power law index for Cross fluids are in the denominator and shear thinning Cross fluids have a power law index n > 1.

Herschel-Bulkley model for Bingham plastics

The Herschel-Bulkley model is the only model in fluent that takes yield stress into account [35]. The version of Herschel-Bulkley model found in most literature is similar to the Power law model above a shear stress threshold value τ_0 and acts as a solid or a highly viscous fluid beneath.

In Fluent version 12, Ansys has changed the formula for calculating the shear stress into:

$$\mu = \frac{\tau_0}{\dot{\gamma}} + K * \left(\frac{\dot{\gamma}}{\dot{\gamma}_c}\right)^{n-1} \text{ when } \tau > \tau_0$$

Eq. 3-6

This is due to a change of the Herschel-Bulkley model from the standard formulation to a Herschel-Bulkley for Bingham plastics formulation which approaches a Newtonian viscosity behaviour as the shear rate increases.

When flowing in pipes the shear stress will be below the critical yield stress in the centre of the pipe causing the flow to act as a solid in the centre of the pipe. Similarly in a two fluid case with a non yield stress fluid flowing in the centre of the pipe the shear stress near the wall may be to low causing the yield stress fluid to solidify.

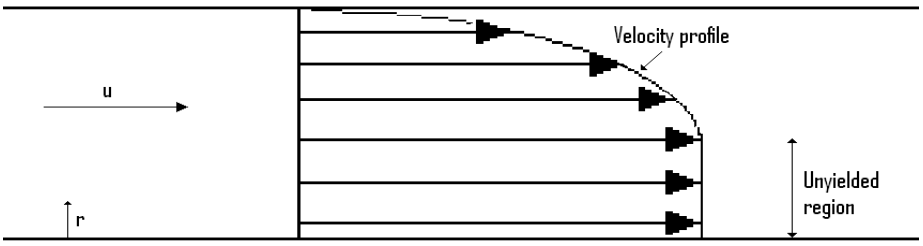

Figure 12 Velocity profile for Herschel Bulkley fluid in pipe

The maximum velocity of the standard Herschel-Bulkley model velocity profile can be calculated from solving ∅ from equation 3-6 and inserting it in equation 3-7 [27].

$$Q = \pi R^3 n \left(\frac{\tau_0}{K * \emptyset}\right)^{\frac{1}{n}} (1-\emptyset)^{\frac{n+1}{n}} \left\{\frac{(1-\emptyset)^2}{3n+1} + \frac{2\emptyset(1-\emptyset)}{2n+1} + \frac{\emptyset^2}{n+1}\right\}$$

Eq. 3-7

$$V_{max} = \frac{nR}{n+1}\left(\frac{\tau_0}{K * \emptyset}\right)^{\frac{1}{n}} (1-\emptyset)^{\frac{n+1}{n}}$$

Eq. 3-8

Viscosity of water and product mixtures

When the product is dissolved into the water it is likely to become an emulsion similar to milk. Multiple studies of the effect of dissolved product in water on the viscosity have been carried out.

It has been showed that the particle size of the dissolved phase has no impact on the viscosity of the mixture which is only a function of the dissolved fluid fraction and viscosity ratio between the continuous and the dissolved fluid [28].

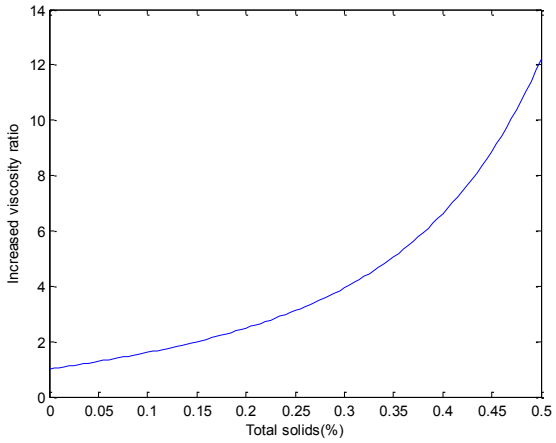

Figure 13 Plotted data for the Yaron and Gal model at high viscosity ratio between fluids

One of the most accurate formulas for the viscosity of emulsions is the Yaron & Gal-Or model which relates the relative viscosity $\eta_r = \frac{\mu_{mixture}}{\mu_{water}}$ to the volume fraction φ and viscosity ratio κ, the formula is large and the results for a large viscosity difference between the fluids are plotted in figure 13 [28].

Experimental studies of the variation of viscosity in a yoghurt water mixture with yoghurt fraction have showed a Newtonian behaviour of the mixture [29]. At a total solid fraction of 6.5 % which is approximately 50 % yoghurt and 50 % water, the viscosity of the mixture had only increased with 50 % and no non-Newtonian effects were present[29]. This corresponds well with results obtained from the Yaron and Gal-Or formula for $\kappa=\infty$ which estimated the viscosity increase to 40 %.

Slip

Slip is a common fluid behaviour in food processing applications[27]. It is not a material property and happens when a thin film of low viscosity forms between the fluid and solid common for gels and suspensions. In the cases where slip is assumed to be present in the

product it is accounted for by the standard Mooney method which assumes a linear relationship between the slip velocity and the wall shear stress [30]. Typical values are for yoghurt 0.0024 m/Pas [31].

3.3 Turbulence

At low velocities, the flow can be characterized as laminar and can accurately be described by the governing equations listed above. As the velocity increases the ratio between inertial and viscous forces will increase and eventually a transition into turbulence will take place in the flow. The ratio between inertial and viscous forces is called Reynolds number and is for pipe flow defined as $Re_D = \frac{DU\rho}{\mu}$. For pipe flow this critical ratio is ~2300[32]. In the laminar flow the viscous forces are dominant and will damp out any small perturbation, in the turbulent flow however the perturbations are being amplified resulting in a chaotic flow.

Because in a laminar flow, the viscous forces damp out any fluctuation, the discretized version of the governing equations give accurate results. If the flow instead is turbulent and the CFD solver only solves the governing equations for a mean average in time velocity and pressure field nonlinear parts of the Navier Stokes equation will not be modelled. To understand what impact that has on the results the Navier Stokes equations can be re written with the use of Reynolds decomposition.

When Reynolds decomposing the velocity, the velocity U_i is separated into an averaged component $\overline{U}_i$ and a fluctuating component u'_i.

$$U_i = \overline{U}_i + u'_i$$

Eq. 3-9

If the Navier Stokes equations are rewritten and averaged a new form of the Navier Stokes equations, the Reynolds averaged Navier Stokes equations is derived.

$$\rho\frac{\partial \bar{u}_i}{\partial t} + \rho\frac{\partial \bar{u}_i\bar{u}_j}{\partial x_i} = \rho g_i - \frac{\partial \bar{p}_i}{\partial x_i} + \mu\left(\frac{\partial^2 \bar{u}_j}{\partial x_i \partial x_j}\right) - \rho\overline{u'_i u'_j}$$

Eq. 3-10

This equation differ from the standard Navier stokes equation by the addition of 6 Reynolds stresses $\overline{u'_i u'_j}$. Since no new equations have been derived the equation system has 6 more unknowns than equations and there is a closure problem.

The most common method for closure of the RANS equations is by using the Boussinesq eddy viscosity approximation. The Boussinesq eddy viscosity approximation assumes that the turbulent stresses can be approximated by a turbulent viscosity. The Reynolds stresses in the Navier-Stokes equations can then be replaced by an effective viscosity which can be added to the molecular viscosity to create a effective viscosity to replace the molecular viscosity in the RANS equations.

Various methods for estimating the turbulent viscosity has been developed but the most common are the k-epsilon methods. In the standard k-epsilon model the turbulent viscosity is

assumed to be a function of density ρ, turbulent kinetic energy k, turbulent dissipation ε and a model constant C_μ.

$$\mu_t = \rho C_\mu \frac{k^2}{\varepsilon}$$

Eq. 3-11

The turbulent kinetic energy and turbulent dissipation in each cell is calculated from two additional transport equations.

$$\frac{\partial}{\partial t}(\rho k) + \frac{\partial}{\partial x_i}(\rho k u_i) = \frac{\partial}{\partial x_j}\left(\mu + \frac{\mu_T}{\sigma_k}\frac{\partial k}{\partial x_j}\right) + \mathrm{P}_k + P_b - \rho\varepsilon - Y_M$$

Eq. 3-12

$$\frac{\partial}{\partial t}(\varepsilon\rho) + \frac{\partial}{\partial x_i}(\varepsilon\rho u_i) = \frac{\partial}{\partial x_j}\left(\mu + \frac{\mu_T}{\sigma_\varepsilon}\frac{\partial \varepsilon}{\partial x_j}\right) + C_{\varepsilon 1}\frac{\varepsilon}{k}(P_k + C_{3\varepsilon}P_b) - C_{2\varepsilon}\rho + C_{2\varepsilon}\rho\frac{\varepsilon^2}{k}$$

Eq. 3-13

Where P_k is the production of turbulence in the flow and its formula is model specific. P_b is the production of turbulence from buoyancy in the flow which is nonexistent in a system without heat transfer. Similarly Y_M is a term that takes dilation dissipation into account which is caused by compressibility and is thus zero in this case. σ_k, σ_ε, $C_{\varepsilon 1}$, $C_{\varepsilon 2}$ and $C_{\varepsilon 3}$ are model constants.

Fluent offers three different full turbulence k-epsilon models and an additional 6 low Reynolds number k-epsilon models.

The 3 different k-epsilon models for fully developed turbulence are standard k-epsilon, RNG k-epsilon and Realizable k-epsilon. The low Reynolds k-epsilon models differ from the fully turbulent Reynolds number models as they do not use wall functions and instead resolve the wall function by damping various terms in the k-epsilon transport equations and adding source terms, most notably the turbulent viscosity. An example is the Abid model which multiplies the turbulent viscosity equation 3-8 with a function $f_\mu = (1 + 3.4/\sqrt{Re_t})\tanh\left(\frac{y_+}{80}\right)$ to approximate the near wall behaviour [33].

Other two equation turbulence models are the k-omega models which have a similar form to the standard k-epsilon but the transport equation for the dissipation has been replaced by a dimensionless dissipation omega.

A more accurate method for modelling the turbulence is by Large Eddy Simulation (LES) which improves the turbulence modelling by solving the Navier Stokes equations after being filtered by the mesh. Small scale motions are then not being resolved and needs to be modelled. This way the method resolves a larger portion and models less of the turbulence.

The turbulence also becomes more homogenous with a decrease length and time scale making increasing the accuracy of the modelling.

Boundary layers

The near wall behaviour of turbulent flow is very complex and the turbulence models need special treatment to accurately capture boundary layers. When describing the velocity boundary layer it usually divided into three different layers which thickness is being described by the dimensionless wall distance $y^+ = \frac{u_t y}{\nu}$ where u_t is friction velocity $u_t = \sqrt{\frac{\tau_w}{\rho}}$.

Near the wall the turbulence is being damped out and only molecular viscous forces are present, this layer is referred to as the viscous sublayer and is $y^+ = 5$ thick. The velocity in the viscous sublayer is approximated by the formula $\frac{\bar{U}}{u_t} = y^+$. Outside the viscous sublayer there is a buffer layer which is $y^+ = 55$ thick in which both molecular viscosity and turbulence is important. Outside the buffer layer the fully turbulent region begins. The thickness of the fully turbulent layer depends on the Reynolds number of the flow. The velocity in the fully turbulent region is described by a logarithmic function:

$$\frac{\bar{U}}{u_\tau} \approx 2.5 \ln y^+ + 5.45$$

Eq. 3-14

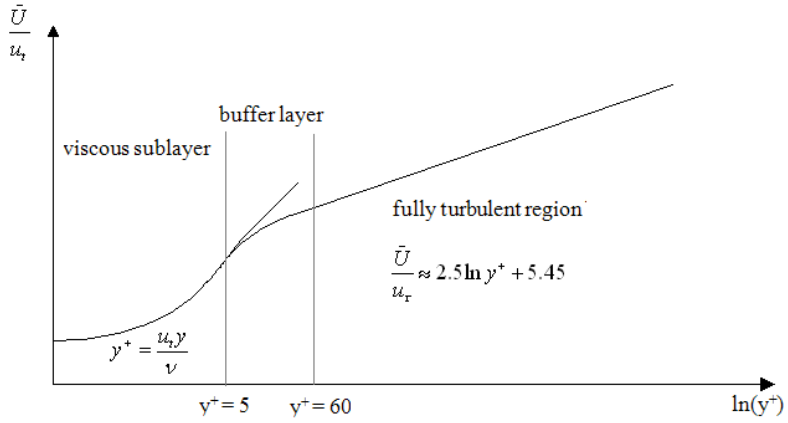

Figure 14 The turbulent boundary layer

Various methods applied by the turbulence models to capture the near wall behaviour has been developed.

To conserve computational resources, the near wall behaviour is usually calculated from wall functions or wall treatment. This is true for the k-epsilon models while the low Reynolds k-epsilon models utilizes damping functions near the wall.

When using wall functions the viscous sub layer is not resolved and is instead calculated from empirical formulas. This removes the need for increased mesh resolution near the walls and saves computer power. The wall functions are derived for high Reynolds number flow and have poor accuracy for low Reynolds number flow.

The wall treatment method separates the boundary layer into two layers. In the outer layer the flow is considered unaffected by viscosity and the standard turbulence model is applied. In the inner layer the standard turbulence model is blended with a damped turbulence model. For this method to give accurate results, a high near wall grid resolution is required and at least one cell needs to be within the viscous sub layer.

Velocity profile in pipe

An approximate method that describes the fully developed velocity profile for turbulent flow is the power law method describing the mean axial velocity as a function of the maximum velocity, radius and an integer m=$\frac{1}{\sqrt{f}}$ [42].

$$\overline{U} = \overline{U}_{max} * \left(\frac{R-r}{R}\right)^{1/m}$$

Eq. 3-15

For Reynolds number in the range 4000-10^5 the friction factor in smooth pipes can be estimated as f=0.316*$Re^{-1/4}$ [32].

The maximum velocity in fully developed turbulent pipe flow can be calculated from $\overline{U}_{max} = \overline{U} * (1 + 1.3\sqrt{f})$ resulting in maximum velocities in the water phase of 1.23 times the mean velocity for Reynolds number 10^4 [32]. For laminar flow the maximum velocity is twice as high as the average velocity.

3.4 Computational methods

Computational fluid dynamics or CFD involves using computational methods to solve the governing equations listed above. Since there are very few analytical solutions to the Navier-Stokes equations and they only exist for very simple cases there is a need for numerical methods to solve them. The most common methods are the finite difference method, the finite element method and spectral methods.

The CFD software chosen to calculate the displacement behaviour is Fluent. Fluent uses the finite volume method which is based on the finite difference method to discretize the governing equations. The finite volume method is a good choice because the sum of fluxes entering and leaving the control volume equals the change of the property of the control volume and thus it is conservative. A second advantage is that it can easily be applied to arbitrarily shaped cells.

In the finite volume method the flow domain is divided into a large number of control volumes called cells which together form a mesh. An integrated version of the governing equations is later being solved by integrating along the surfaces and throughout the cells volume. In the centre of a cell there is a node which is where certain properties of the cell is stored.

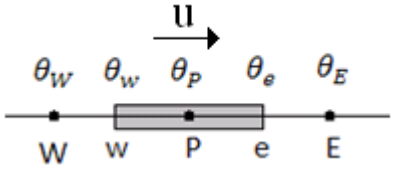

Figure 15 The cell surrounding node P

When discretizing the governing equations for the finite volume method a method is needed to evaluate the transported properties of the flow at cell faces. The simplest method is the central differencing scheme which simply calculates the property as the average of the two nearest perpendicular nodes $\theta_e = \frac{\theta_E + \theta_P}{2}$ where capital letters indicate node values and lower case letters are face values.

Because the properties at the cell face is likely to be more affected by the values upwind of the cell face than those downstream the differencing schemes are usually being weighted to take the upstream values more into account. The simplest upwind method is the first order upwind which estimates the property a face e as the property in upstream node P, $\theta_e = \theta_P$ which is only first order accurate. To increase the accuracy second order upwind and third order QUICK schemes can be used. The QUICK scheme interpolates the value at face e from $\theta_e = \frac{3}{8}\,\theta_E + \frac{6}{8}\,\theta_P - \frac{1}{8}\,\theta_W$

A higher order scheme increases the accuracy and reduces diffusion but usually leads to slower convergence and larger equations to compute.

A limiting factor when using explicit solvers is the time step size which is limited by a dimensionless Courant number. The Courant number is the difference between the distance the flow will travel during a time step and the size of the cells $C=\frac{\bar{U}\Delta t}{\Delta x}$. A Courant number larger than 1 indicate that the flow will travel further than one cell during a time step causing the simulation to become unstable. This is the CFL condition, which is only relevant when using explicit methods. Using implicit methods, which are unconditionally stable, one may use larger time step sizes, however with the potential loss of time accuracy.

Mesh

The mesh is a group of cells that together form the flow domain. There are two basic types of meshes structured and unstructured. Structured meshes are often Cartesian, block based or body fitted and are built up by hexahedral cells. While the unstructured meshes usually consist of tetrahedral. Tetrahedral cells have a lower order of accuracy than hexahedral cells and thus generate more numerical diffusion. Hexahedral cells are also larger which reduces the cell density. Usually structured meshes also converge faster but it might not be an option for complex geometries.

Special care must be taken near the walls where the boundary layer is developed and the requirements for a fine mesh are much higher.

Pressure velocity coupling

The solution of the discretized governing equations is being complicated by the fact that for incompressible flow there is no coupling between the pressure and velocities in the continuity equation. Another problem is the risk of achieving a checker solution. To overcome these problems the velocity must be evaluated at cell faces and either a staggered grid or interpolation can be used.

When using a staggered grid the velocity information is being stored at the cell faces while other quantities such as pressure and mass fraction is being stored at the cell centre and the equations are being solved by a decoupled algorithm. The other option is to calculate the velocities at the cell faces by an interpolation such as Rhie-Chow and solving the continuity and momentum equation in a coupled way. This is popular for compressible and high Mach number flow where the staggered methods have slow convergence.

Fluent offers 4 different algorithms for staggered grids. SIMPLE, SIMPLER, SIMPLEC and PISO.

All of the algorithms are based on the standard SIMPLE(Semi Implicit Method of Pressure Linked Equations) algorithms which is a semi implicit algorithm where an initial guess is made and corrections are being estimated. The SIMPLER, SIMPLEC and PISO algorithms are either modified SIMPLE algorithms or have additional corrector steps.

The PISO(Pressure Implicit with Splitting of Operators) was developed for non iterative transient incompressible flow calculations and is generally recommended for transient simulations.[34]

3.5 Multiphase flow

When modelling miscible multiphase flow there are two categories of methods, either Lagrangian or Euler-Euler. The Lagrangian method is used for tracking individual particles and estimating trajectories and is very computationally expensive for multiple particles. The Eulerian methods are used for solving flow fields with multiple components and do not track individual particles. For displacement processes Eulerian methods must be used.

A useful dimensionless number for determining the slipping between phases is the Stokes number which is the ratio between system and particle response time [35].

$$St = \frac{\rho_d d_d^2 V_s}{18 \mu_c L_s}$$

Eq. 3.16

Where subscripts d and s denote the dispersed phase and the system, respectively. When St < 1, the dispersed particles are strongly coupled with the continuous fluid causing them to follow closely with the movements of the main flow. For St > 1the particles are too large or too heavy to follow the flow of the continuous phase and should be modelled independently.

There are 2 Euler-Euler methods available in Fluent. Eulerian and mixing model. Another method for multiphase flow is the Volume of fluid (VOF) method.

Volume of fluid

The VOF model is an interface capturing method used to model immiscible fluids. It does ideally not allow any mixing between the phases but because of numerical diffusion the phases will mix. This is a problem with this method when applying it on the displacement processes as it takes a long time for the interface to travel from the entrance to the outlet causing much numerical diffusion on the way if the VOF formulation is not carefully chosen.

The VOF methods are solving one set of the governing equations plus a volume fraction convection equation and vary the fluid properties linearly with the volume fraction distribution in the cells.

The volume fraction convection equation solved is:

$$\frac{1}{\rho_q}\left[\frac{\partial}{\partial t}\left(\alpha_q \rho_q\right) + \nabla * \left(\alpha_q \rho_q u_{iq}\right) = S_{\alpha_q}\right]$$

Eq. 3-17

Where p is the primary and q is the secondary phase. α_q is the volume fraction and can either be:

$\alpha_q = 0$: No secondary fluid q in the cell.
$0 < \alpha_q < 1$: The cell is in the interface between two phases.
$\alpha_q = 1$: The cell only contains secondary fluid q.

The volume fraction convection equation is only solved when $0 < \alpha_q < 1$.

Fluent offers 7 different VOF formulations:

Geometric-Reconstruction
Donor acceptor
Modified HRIC
CICSAM
Quick
Second order upwind
First order upwind
Out of these Geo-reconstruct, CICSAM and Donor Acceptor are only available for explicit formulation.

The implicit VOF formulations should only be used for steady state and transient flow where an eventual final steady state solution is achieved [35]. Only first order discretization in time is available for VOF calculations in fluent. The explicit formulations are only available for transient solutions.

Because the interface is captured by advection of a volume fraction quantity solved from a convection equation, it is sensitive to numerical diffusion caused by the differencing scheme. The most simple of the VOF formulations uses standard discretization of the convection equation. The common first and second order upwind and QUICK discretization methods are available but also specially developed higher order schemes to minimize the diffusion can be used.

Upwind schemes are diffusive but bounded and stable while downwind schemes are compressive of the interface but unbounded. Fluent offers three upwind based discretization methods out of which QUICK is by far the most accurate.

To solve the problems with upwind and downwind discretizations, complex methods which combines upwind and downwind interpolation has been developed [34]. Such methods available in fluent are CICSAM (Compressive interface capturing scheme for arbitrary meshes) and HRIC (High Resolution Interface Capturing). The CICSAM was developed by Ubbink [36] and is a high resolution differencing scheme. The CICSAM is recommended for flows with high viscosity ratios and is almost as sharp as Geometric reconstruction [35]. Another high resolution differencing scheme is HRIC which is more accurate than QUICK but less accurate than CICSAM.

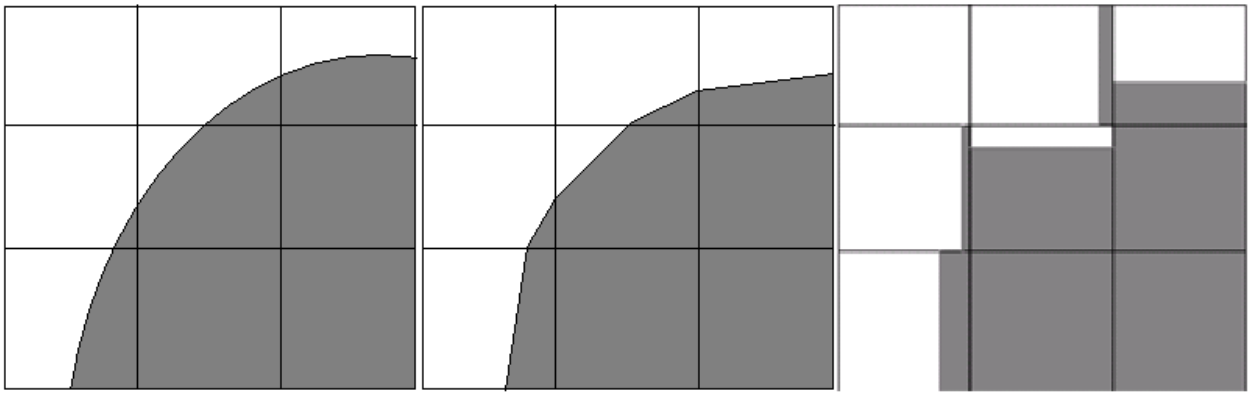

Figure 16 Geometric reconstruction scheme (left), Donor acceptor scheme (middle) and exact phase front (right)

There is also a more complex group of methods estimating an interface between the fluids and using this information to compute advection. This group of methods are either donor acceptor or geometric reconstruction based.

The Geometric-Reconstruction scheme is the most accurate of the VOF formulations and assumes a sharp interface between the two fluids and uses the information about the interface when determining the advection between cells. The only reconstruction based method in Fluent is the piecewise linear interpolation capturing method estimating the interface as a series of straight lines connected at the cell faces and in each time step attempt to reconstruct it.

The donor acceptor scheme estimates an interface from volume fraction values upstream and downstream of the interface and uses this information to calculate the transport of volume fraction from a donor to an acceptor cell to minimize numerical diffusion. The interface is simplified as either vertical or horizontal [34][35]. The method uses downstream values making the method unbounded causing volume fractions lower than 0 and higher than 1. Methods such as controlled downwinding and bondedness and availability criteria's are needed to generate physical results [34].

In Fluent no options for boundary conditions at the fluid-fluid interface is available. The physics of the flow near the interface is uncertain and the interface is often treated as a wall. Simulations validated by experiments show that approximating the near fluid interface with wall functions for rough walls yields good results. [37]

When tracking an interface between to immiscible fluids there are many alternative methods to VOF which are not supported by Fluent. Usually the methods are divided into interface capturing or interface tracking methods. The VOF is a interface capturing method, other common such methods are the Marker and Cell (MAC) and the Level Set Method. The MAC method is an interface capturing method which tracks the interface by tracking the movement of mass less particles in the fluid. The model is very accurate for complex phenomenon's and can capture phenomenons such as wave breaking. Because it involves tracking of particles it is compared to VOF computationally very expensive and is commonly only used for 2D flow

[34]. Unlike the interface capturing methods which track the transport of the volume fraction and only estimates the interface for calculating advection, the interface tracking methods are tracking the interface and the volume fraction can only be 1 or 0 and is determined by what side of the interface the cell is [34]. One such method is the Markers on Interface which is similar to MAC and tracks mass less particles which capture the interface. The method is thus able to capture small scale motions in the interface. Downsides of the method are its inability to handle breakage and merging of interfaces and that it is not volume fraction conservative.

When modelling non Newtonian fluids the non Newtonian fluid should be chosen to primary for most accurate results.

Eulerian

The second Euler-Euler method available in fluent is the Eulerian Method. In the Eulerian method one set of the governing equations are solved for each of the phases and an extra transport equation for each extra phase. The phases share pressure field and the coupling between the phases are achieved by additional forces in the momentum equations. These forces are calculated from the slip velocities between the separate phases in each cell. When calculating the turbulence a single or multiple turbulence equations can be solved but for stratified flow a single turbulence model is enough [35]. Because for a two phase flow twice as many equations need to be solved Eulerian is the most computationally heavy of the Euler-Euler methods but also more accurate than mixing model and species transport. It does however assume mixing between the phases and cannot capture an interface for immiscible fluids like VOF.

Multiple methods for calculating the forces between the phases are available and they all assume that one phase is dispersed in another. The force is calculated from drag laws based on an expected diameter of the dispersed fluid and the slip velocity. Only one model in fluent, the symmetric model is applicable for flows when both phases are primary and dispersed in different parts of the flow.

Mixture model

In the mixing model one set of the governing equations are solved and an additional volume fraction equation for each additional phase. The mixture model assumes a strong coupling between the phases and that they share the same velocity field and is only valid when the difference in velocity is very small. The dispersed fluid is only expected to make short slip movement and never develop its independent velocity field. The mixture model attempts to estimate the slip each time step based on the drag functions and the acceleration fields in the flow.

Species transport

Species transport in a homogenous multi component model which assumes that all the species are mixed on a molecular level and does not attempt to calculate any slip between the phases. Instead any mixing is assumed to come from molecular and turbulent diffusion. One set of

governing equations plus a species transport equation is solved. This model can also be used combined with VOF.

3.6 Mass transfer

As water displaces a fluid some mixing between the phases is to be expected. This mixing between the phases may be caused by molecular diffusion, turbulent diffusion and erosion. The molecular diffusion of water in yoghurt has been estimated to be in the range 10^{-9} to 10^{-10} m^2/s [38][39]. This will most likely have a minimal effect on the displacement process which is indicated by the results present in figures 52 and 54 showing continuously growing residual films for product 1.

The second form of mass transfer is the turbulent diffusion created by the turbulent eddies in the flow spreading the product. Because only the water phase is assumed to be turbulent this will not have a large effect on the mass transfer rate between the phases as the molecular diffusion is needed for transporting the dissolved product out of the viscous sub layer and into the fully turbulent regime. In the case of a turbulent product phase the turbulent diffusion can be assumed to have a large impact on the displacement process as the mass transfer will become very large. The turbulent diffusion is usually considered to vary with the turbulent viscosity in a ratio referred to as the turbulent Schmidt number $Sc_t=\frac{\nu_t}{D}$. The turbulent Schmidt number varies throughout the pipe and decreases near the walls. It is usually being modelled as a constant Sc_t except for the RNG k-epsilon model which uses an analytical formula. Standard values are $Sc_t=0.7$ and values given in literature ranges between 0.4 and 1.1 [40]. Studies of turbulent mass transfer specifically in pipes has shown that an average of $Sc_t=0.625$ works well [43]. This would give an approximate turbulent diffusion of 0.1 m^2/s in turbulent pipe flow in this case.

4 Development of a method

When simulating the displacement process multiple choices for the CFD code needs to be made. The choices discussed in this chapter are the multiphase model, inclusion of mass transfer mechanism, gradient evaluation method, turbulence model, rheology model, grid resolution, VOF formulation, time step size and discretization.

When investigating the various aspects of the method, a case of water displacing a power law fluid (K=5, n=0.35) with the volumetric flow rate of Q=0.00 108 m^3/s in a three dimensional pipe was used when nothing else is stated.

4.1 Mass transfer

Experiments on the mass transfer of a highly viscous dairy product into water indicate that the mass transfer is caused by an erosion process [41]. During experiments on water flowing through a canal of the product there was a mass transfer of the product into the water as long as the shear stress at the interface to the product was above a critical shear rate. When the canal had reached a large enough diameter, causing the shear stress to be reduced, the mass transfer ceased. This indicates that the dominant mass transfer mechanic is erosion of the product into the water and a similar behaviour is expected for product 2, product 1 and other dairy products.

4.2 Multiphase model

The possibility of slipping between the phases was tested for both Eulerian and Mixture model using symmetric drag functions for velocities of 1 m/s in a 6 cm in diameter pipe with a density difference of 37 kg/m^3 between the phases. The Stokes number of the case was St=0.9 for 1 mm large particles and 10^{-6} for 1 μm large particles. This indicate that the coupling between the two phases is very strong and they flow as a single fluid. When simulating the displacement with Eulerian and Mixing model with the symmetric drag function, no slipping between the phases was noticeable until the particle sizes for the dispersed phase was modelled as at least 0.1 mm. This is considerably larger than the size of the dispersed product present in this case. Because the Eulerian and Mixing model are developed for mixing phases there are no numerical schemes for keeping the fluid-fluid interface sharp and the use of these models result in large numerical diffusion and they both have poor ability to capture instabilities unless the mesh is very dense. No sliping between the phases is thus considered and the VOF method for multiphase flow was chosen.

To take mass transfer between the phases into account the VOF formulation was combined with a species transport method where the water phase was modelled as mixed species of product and water with the viscosity determined by Yarons formula plotted in figure 12. The use of mass transfer between the phases did however remove instabilities as information about small perturbations on the interface were lost when the interface was moved. The main problem with implementing the evaporation mass transfer method is calculating the shear stress. As will be discussed in part 4.4 the turbulence modeling is very inaccurate, especially the estimation of the turbulent viscosity. This results in overestimations of the shear stress at

the fluid-fluid interface which leads to an overestimation of the mass transfer. When comparing the shear stresses at the interface calculated by fluent with the estimated shear stresses computed from analytical solutions for pipe flow, the shear stresses calculated by fluent were overestimated by up to a factor 5. Instead a UDF estimating the shear stress from analytical formulas was written and showed reasonable results but it was never used in the final model because as will be discussed in section 5.2 the mass transfer does not have an important role in determining the displacement velocity and very little mass transfer will have time to develop in a 5 meter long pipe.

4.3 Gradient evaluation method

The choice of gradient evaluation method was investigated. The more complex least square cell based method was compared to the faster and better converging Green Gauss Cell Based method when computing the velocity profiles for non Newtonian fluids. The result was also compared to the analytical solution. The Green Gauss cell based method was the fastest and gave best convergence but overestimated the maximum velocity of the profile by more than 3 %.

The biggest problem associated with the Green Gauss method was the poor estimation of the velocity profile in the near wall region where it completely failed to capture the curvature. The least square cell based method overestimated the velocity by less than 0.5 %. Investigation of the viscosity showed that the Green Gauss node method fails to calculate the non-Newtonian viscosity in the near wall region. This causes an incorrect velocity profile near the wall which has effects on the entire velocity profile.

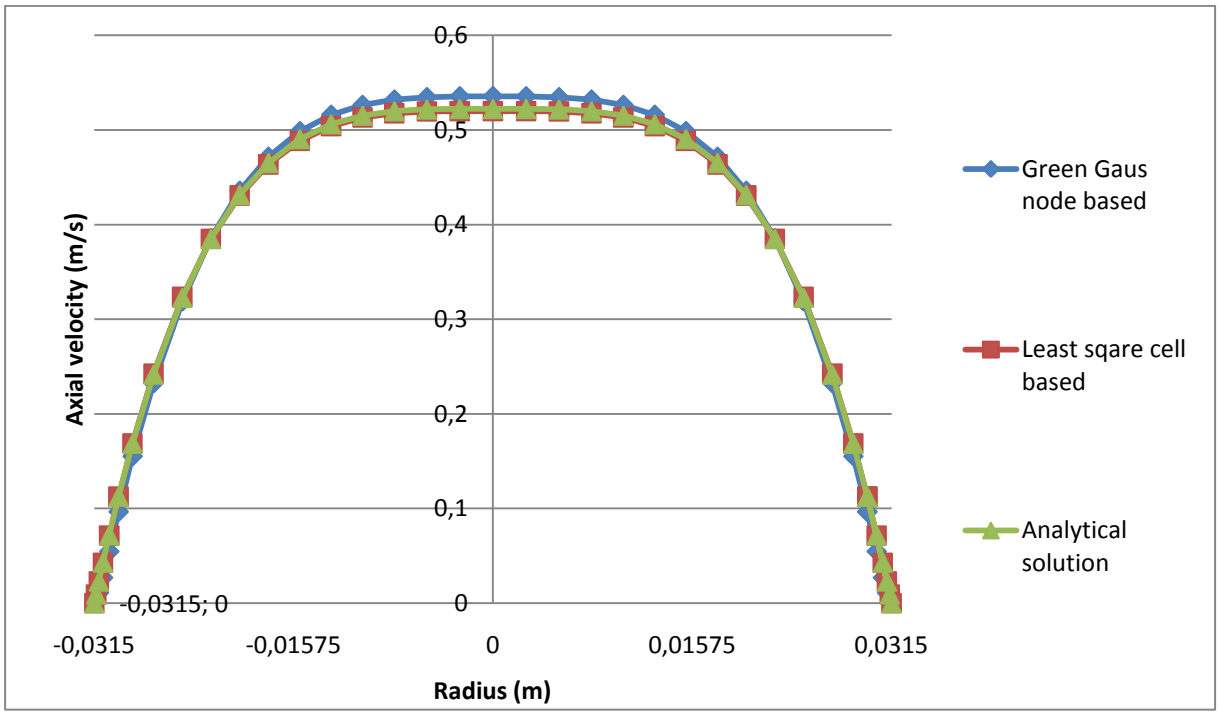

Figure 17 Comparison of power law velocity profiles for least square cell based and Green Gauss node based gradient evaluation.

These problems associated with the Green Gauss node based method were not present for Newtonian fluids.

The least square cell based method was used for all simulations in this paper.

4.4 Evaluation of turbulence models

Near the fluid-fluid interface a boundary layer which is similar to near wall flow is present [37]. This poses a problem when modelling the flow using CFD software as no wall treatment options are available for a fluid-fluid interface. Nor is the mesh adequately resolved to capture the large velocity gradients in the velocity profile present near the interface. The biggest difficulty associated with choosing a turbulence model in this case is to choose one that minimises the errors associated with the assumed near wall behaviour at the fluid-fluid interface. In the case of turbulence in the displacement fluid, the laminar non-Newtonian fluid will cover most of the walls and thus prevent the turbulent fluid from being exposed to the enhanced wall treatment boundary condition.

The result is an overestimation of the turbulent viscosity ratio and a failure to capture the turbulent velocity profile. Instead of a maximum velocity about 20% higher than the mean velocity, the simulations yield a maximum velocity up to 60 % higher than the mean velocity. Also the turbulent viscosity ratio is heavily overestimated by a ratio up to 5.

To estimate how well the various turbulence models could capture the velocity profile, the flow in a 3 meter long axisymmetric pipe with 4 cm inner diameter was simulated. The inlet velocity used was 0.5 m/s and the walls were modeled as smooth. The mesh had a resolution of 44 cells across the diameter. The standard k-e, k-e RNG, k-e Realizable, k-w, k-w ssl, k-w ssl low Re and 3-d RNG turbulence models were investigated. The results are shown in figure 18 which show that they all capture the velocity profile well as is expected.

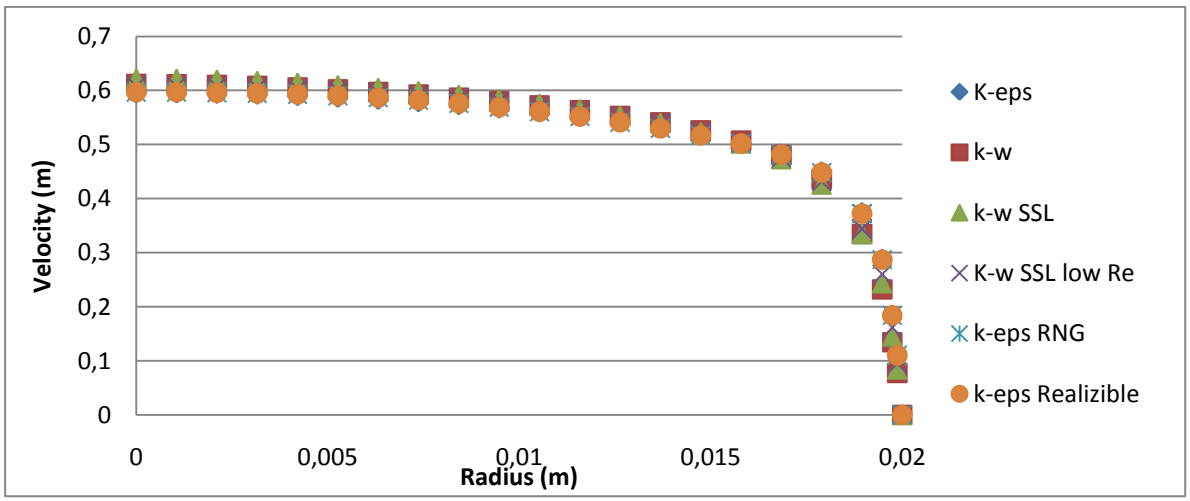

Figure 18 Velocity profile for various turbulence models

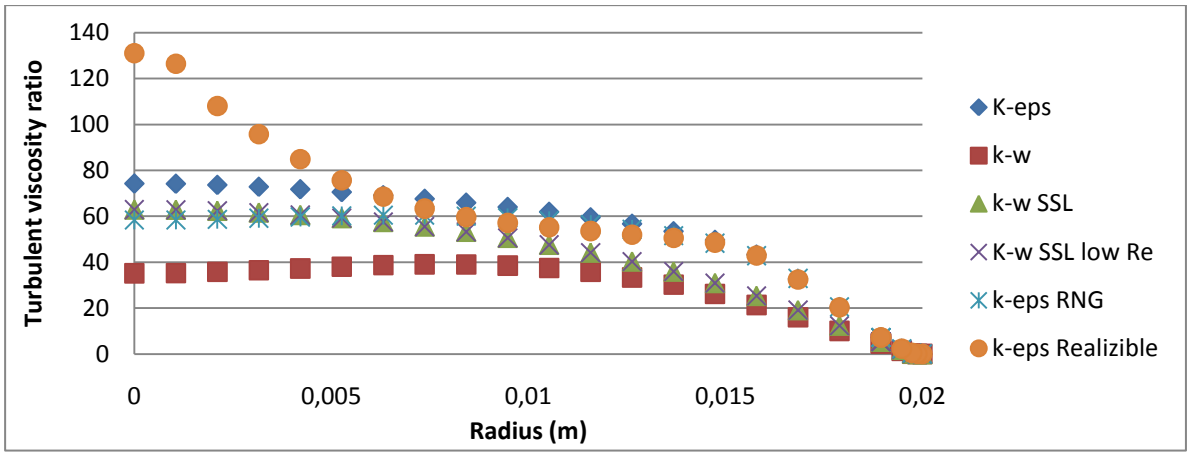

Figure 19 Turbulent viscosity ratio for various turbulence models

These results were later compared to similar simulations conducted in a pipe with a stationary non-Newtonian fluid covering the walls. Through the stationary fluid a 4 cm in diameter axisymmetric canal was created through which water was flowing at a mean velocity of 0.5 m/s. The purpose of this was to simulate how well the turbulence models could capture the turbulent velocity profile of pipe flow when no wall treatment was present.
6 different low Reynolds number k- epsilon models were tested for turbulent viscosity ratio and velocity profiles. Model 1 did not converge and was excluded.

The 6 low Reynolds models tested were:

Model 0	Abid
Model 1	Lam-Bremhorst
Model 2	Launder-Sharma
Model 3	Yang-Shih
Model 4	Abe-Kondoh-Nagano
Model 5	Chang-Hsieh-Chen

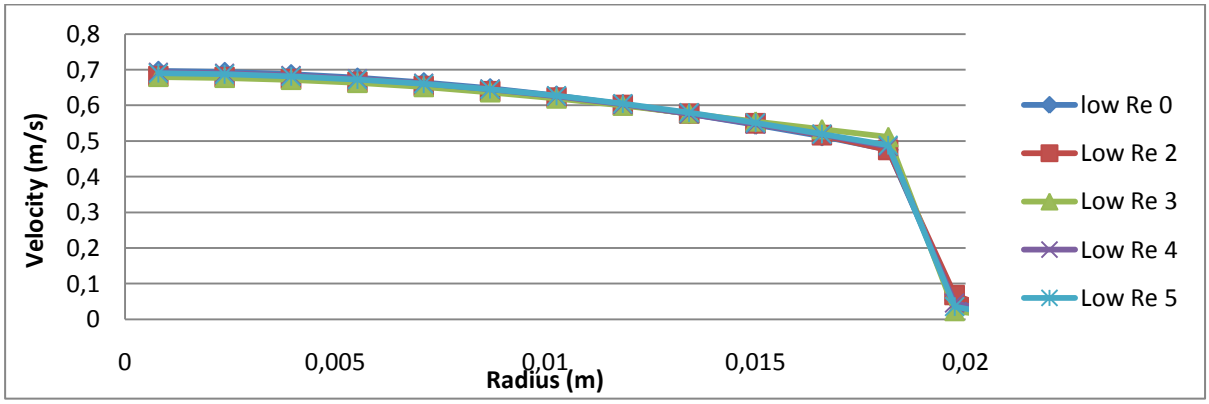

Figure 20 Velocity profile in the canal for the various low Reynolds number models

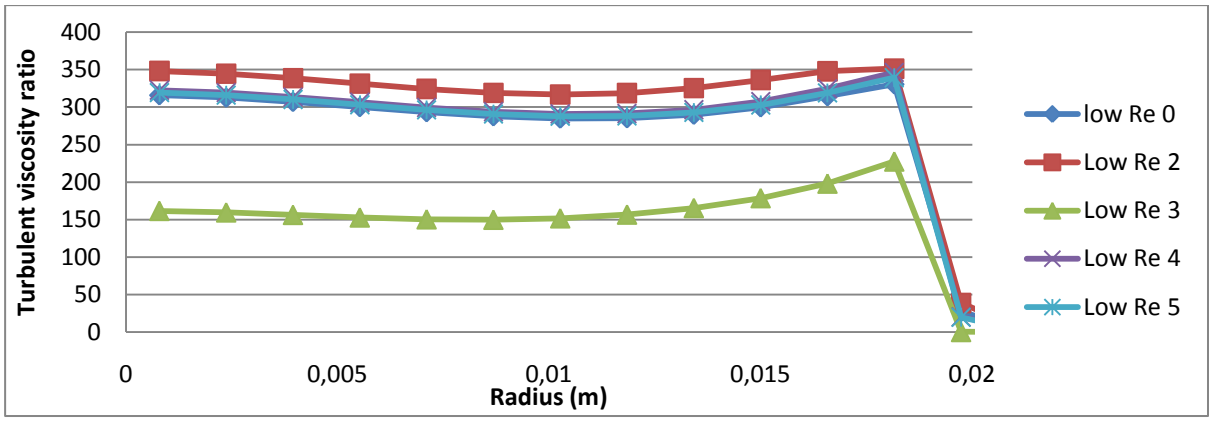

Figure 21 Turbulent viscosity ratios in the canal for various low Reynolds number models

Of the low Reynolds number models model 3 (Yang-Shih) gave the least overestimated turbulent viscosity ratio and best results. Comparison between the full turbulence models available in fluent were also made and plotted in fig 22 and 23 with the exception of k-v2 and SSL model which diverged. Besides the standard models an alternative form of the k-epsilon RNG and a version of the standard k-epsilon model with a few ad-hoc modifications called Kato were simulated. The standard and low Re k-w which had a turbulent viscosity ratio an order of magnitude 10 higher than the other models has also been excluded.

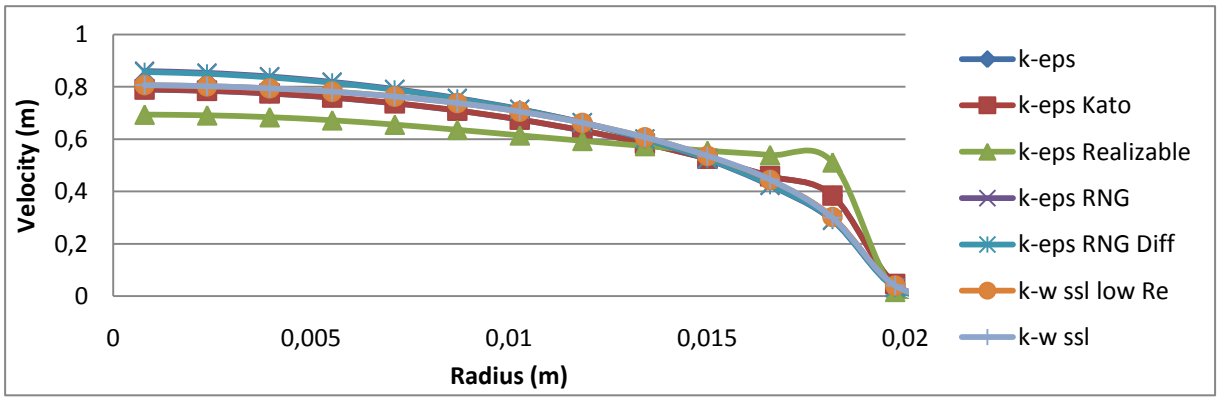

Figure 22 Velocity profile in the canal for different turbulence models

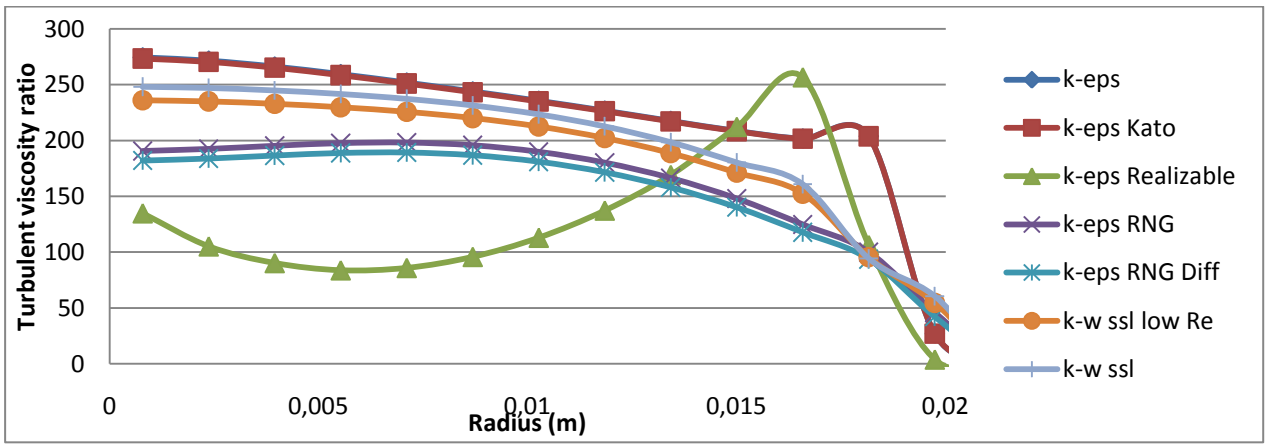

Figure 23 Turbulent viscosity ratios in the canal for different turbulence models

The standard k-epsilon and the k-epsilon Realizable gave the best results and the Kato modifications of the k-epsilon model had no effect in this case. The standard k-epsilon model was also compared to simulations of the standard k-epsilon where the turbulent kinetic energy and a simulation where both the turbulent kinetic energy and dissipation was removed from the non-Newtonian phase. The standard k-epsilon turned out to be the most accurate as can be seen in figure 24.

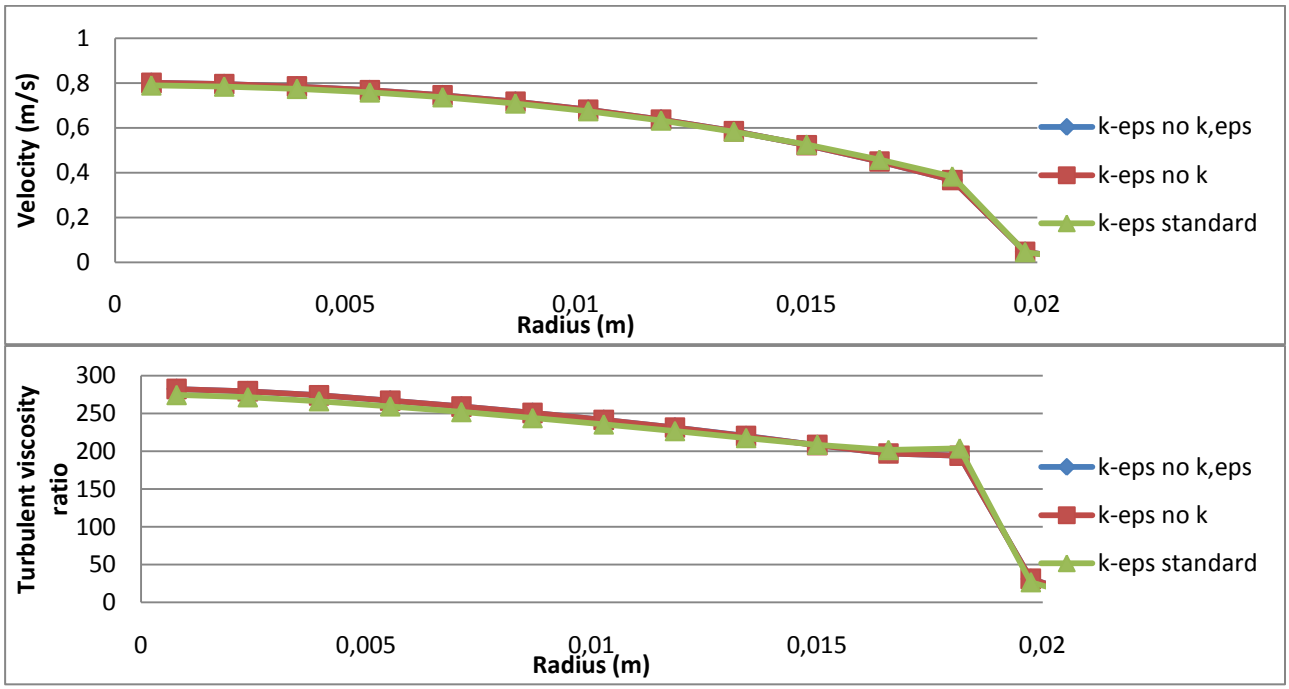

Figure 24 Velocity and turbulent viscosity ratio for various versions of the k-epsilon model

So finally it is between the standard k-epsilon, Realizable k-epsilon and low Re model 3.

Further studies of k-epsilon, low Reynolds model 3 and the k-epsilon Realizable were made at refined meshes.

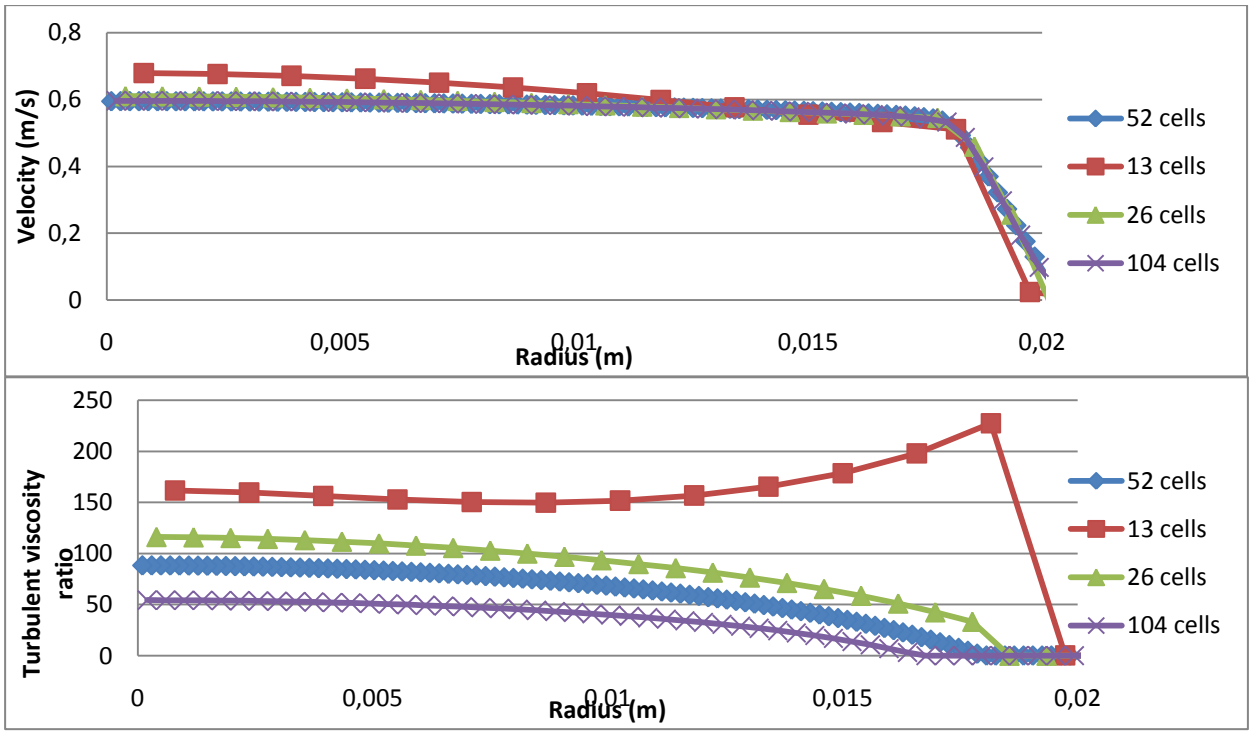

Figure 25 Velocity and turbulent viscosity ratios for low Re k-epsilon model 3 at various mesh densities

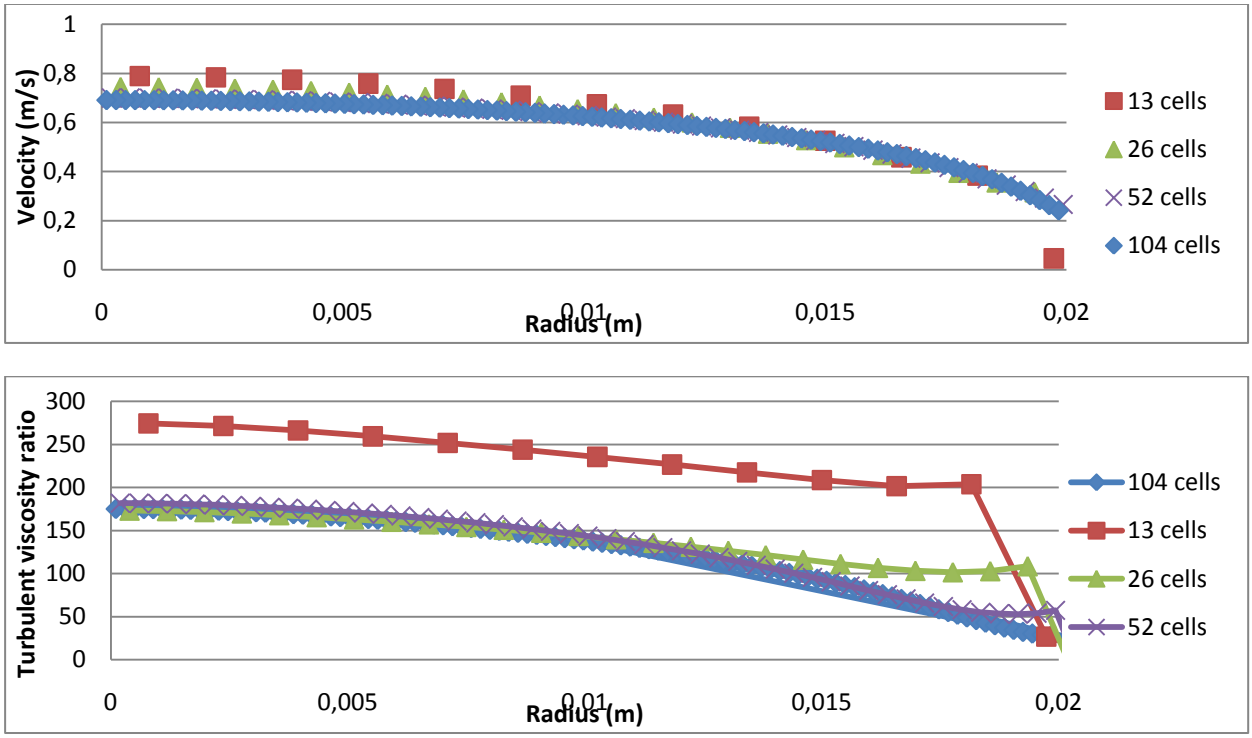

Figure 26 Velocity and turbulent viscosity ratios for the standard k-epsilon model at various mesh densities

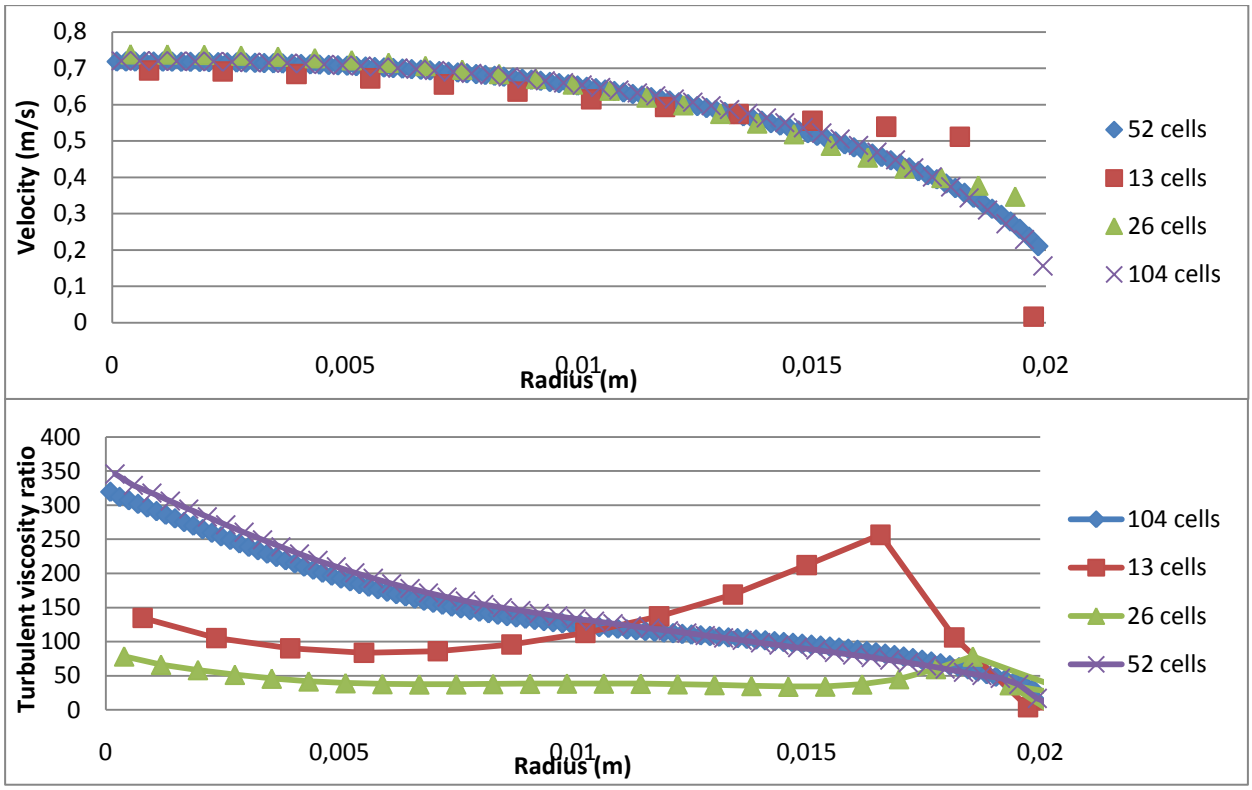

Figure 27 Velocity and turbulent viscosity ratios for the realizable k-epsilon model at various mesh densities

The simulation show an increasingly unphysical behaviour of the low Re model 3 with improved meshing making it unreliable for usage. The turbulent viscosity ratio decreases with an increased mesh density, especially near the wall where there is a growing zone of zero turbulent viscosity ratio.

The k-epsilon Realizable model also show a growing unphysical behaviour as the mesh is refined. When the mesh density increases the velocity profile show an increasingly poor match to the analytical solution.

Of the three the only good model is the standard k-epsilon which approaches the expected solution as the cell density increases.

Turbulence in non-Newtonian fluids

Another turbulence problem is the turbulence in the non-Newtonian fluids. The Reynolds number of a power law fluid is calculated from: $\mathrm{Re}_{\mathrm{pl}} = \frac{\rho V^{2-n} D^n}{8^{n-1} m (\frac{3n+1}{4n})^n}$ [27] and will be in the range 10-200 in the present case. Simulations run show that the non-Newtonian fluids stay in the laminar flow domains for all turbulence models as long as wall treatment is being used. The use of wall function will however generate turbulence in the non-Newtonian fluid which will have an effect on the velocity profile and decrease the accuracy of the simulations and is avoided.

4.5 Viscosity measurements

The following experimental results have been measured by Tetra Pak for the same fluids later used during the experiments:

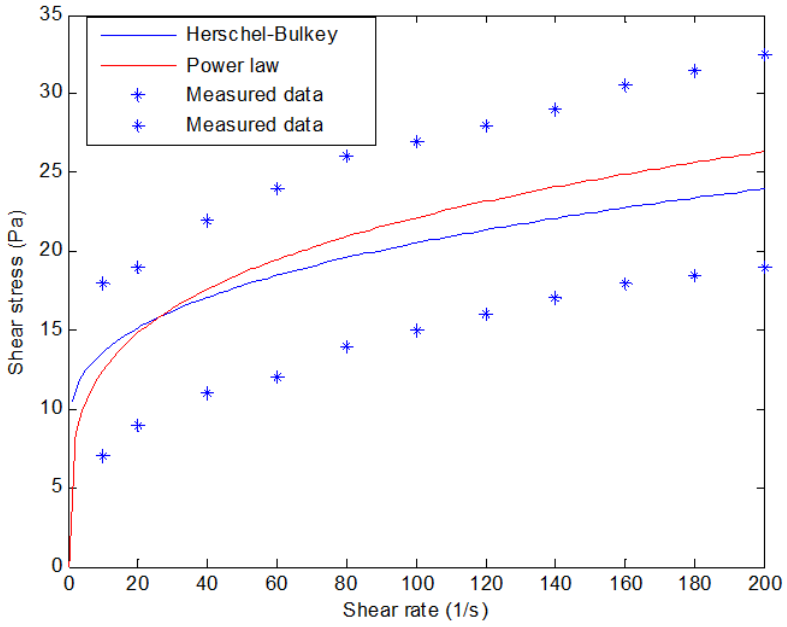

Figure 28 Shear stress-shear rate plot of product 1.

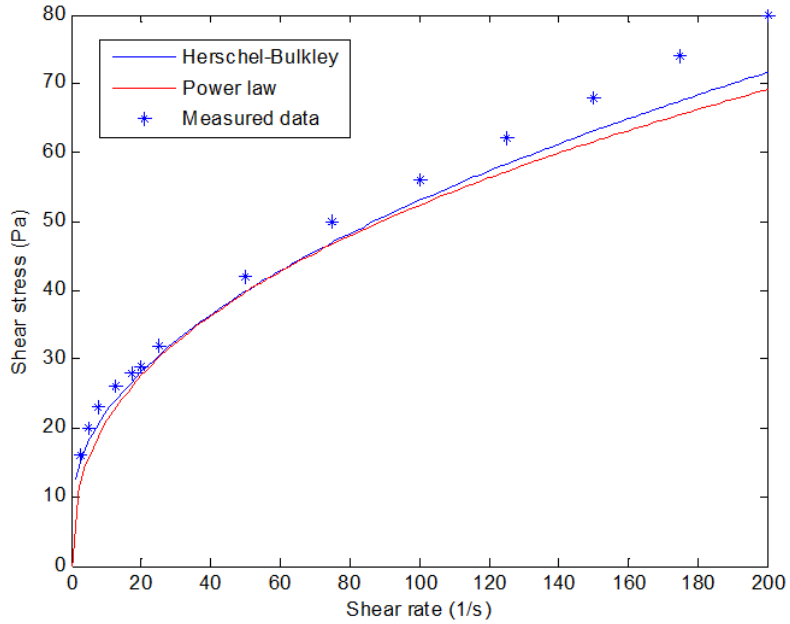

Figure 29 Shear stress-shear rate profile for product 2

Both of the above fluids show signs of thixotropy and possibly yield stresses. Curve fitting a viscosity profile to the product 2 will be somewhat inaccurate since the state of the product 2 in the flow situation is unknown. The shear rate in the applied flow situations will be in the range of 0-200. The curve fitting to the experimental data of both the power law and Herschel-Bulkley models is made for the shear rate range 0-200. The experimental data

matches both the power law and the Herschel-Bulkley model well while the Cross model is unsuitable since it consider the fluid to behave as a Newtonian fluid at low shear rates and a power law fluid at high shear rates while the data indicate a strongly shear thinning behaviour at low shear rates and the fluid approaching a Newtonian behaviour as the shear rate increases. This behaviour conforms well to the behaviour of the Herschel-Bulkley for Bingham fluids model available in Fluent. For product 1 the parameters are fitted it to a medium value between the shear rate increase and decrease curves. This is because the down curves were created after a shearing rate of 1000 1/s and the down curve would be displaced upwards if it would have started from a lower shear rate. For product 2 the shear rate decrease curve was used.

Figure 28 shows plots of the results of the curve fitting for K=5 and n=0.35 for the power law and K=2.5, n=0.35, τ_0=8 Pa, critical shear rate = 1 1/s for the Herschel-Bulkley model.

Figure 29 shows plots of the results of the curve fitting for K=8.3 and n=0.4 for the power law and K=4.5, n=0.5, τ_0=8 Pa, critical shear rate = 1 1/s for the Herschel-Bulkley model to capture the viscosity characteristics of product 2.

Viscosity variations in the mixture

The effect from the increase in viscosity that dissolved product 1 or product 2 has on water has been discussed in section 3.3 where it is clear that the dissolved fluid can have a large impact on the viscosity of the mixture. When comparing it to the large viscosity ratio between the water mixture and the displaced product it is however clear that the change in viscosity will only have a marginal effect on the displacement process and was ignored.

4.6 Mesh

Due to the simple geometry and because of the need to keep the diffusion to a minimum to capture the fluid-fluid interface, a structured mesh built up by hexahedral cells was chosen. To capture the shape of the pipe while keeping the skewing of the cells to a minimum a block based O-mesh was chosen which consisted of a near Cartesian central block surrounded by a body fitted second block. The size of the central block was chosen to minimize the skewing of the cells in the corner of the central block and the aspect ratio variations of the cells in the surrounding block.

Special care was taken to generate fine enough cells near the wall where the cell thickness was chosen to 0.0001 m to keep the y^+ value well below 5 to capture the laminar sub layer which is recommended to capture the boundary layer when using wall treatment. The mesh was generated in ICEM CFD which is a mesh generating software from ANSYS. The final mesh can be seen in figure 30.

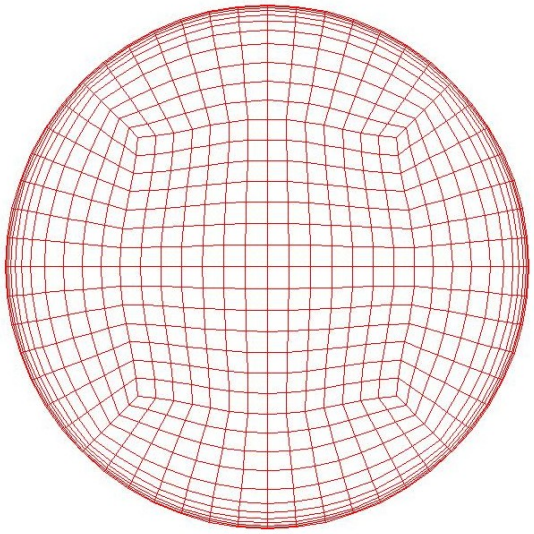

Figure 30 Final mesh choice, 4 cells/cm

The ability to capture instabilities was investigated by simulating the first second of the flow in a 0.0615 meters in diameter pipe for various mesh densities.

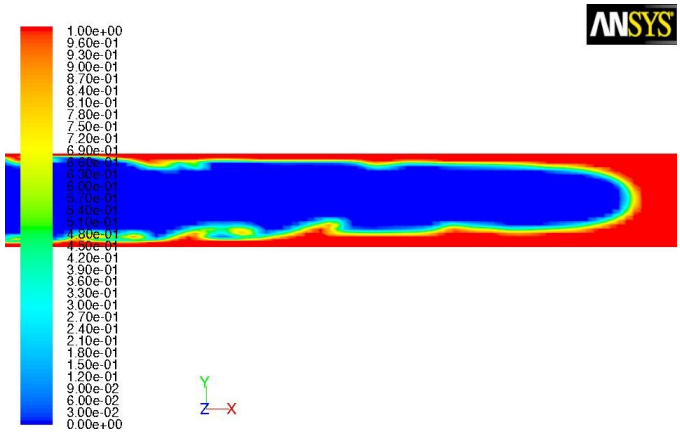

Figure 31 3,5 cells/cm

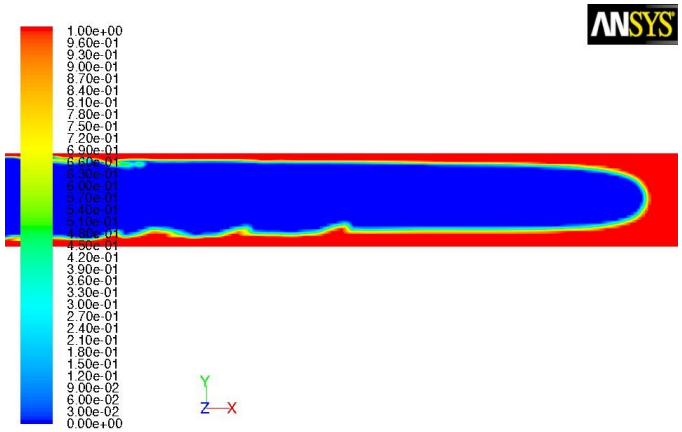

Figure 32 6 cells/cm

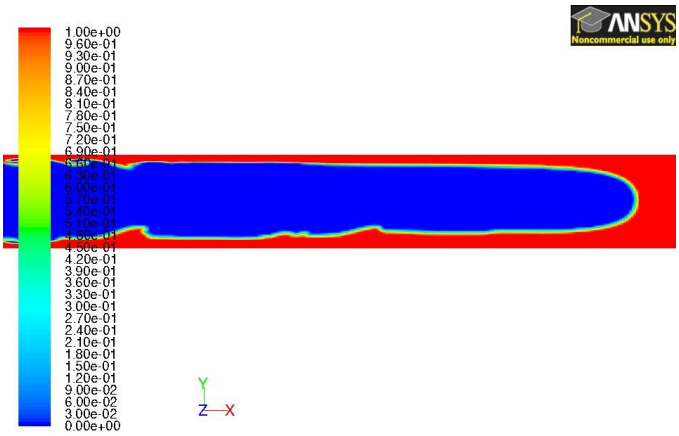

Figure 33 12 cells/cm

The results are shown in figures 31 to 33 where it can be seen that while the 3.5 cells/cm mesh density is enough to capture the instabilities, they tend to grow faster and diffuse into the flow in coarser meshes. In theory a coarse mesh is less accurate and loses information about small scale motions and thus ought to have a poor accuracy when capturing instabilities since they start of as small scale disturbances. This can however not be seen in the simulations.

The use of RANS models which uses a turbulent viscosity tend to have a diffusive effect on the velocity field which removes small scale motions and stabilizes the solution.

The resolution of the mesh used is limited by the requirement for the method to demand reasonable computational resources. A maximum amount of cells was chosen to be limited by 200 000 cells/meter which resulted in a mesh with the density 4 cells/cm which can be seen in figure 30.

Uncertainties about how well the code would handle the instabilities and diffusion in longer pipes and to see what impact the poor turbulence modeling would have on the displacement simulation had to be evaluated and a grid independence test was carried out.

Grid independence was tested by simulating the flow through a 0.063 m diameter pipe for a whole 4 cells/cm pipe and a whole 7 cells/cm pipe. Comparison was made after 6 seconds and the results can be seen in figure 34 and 35.

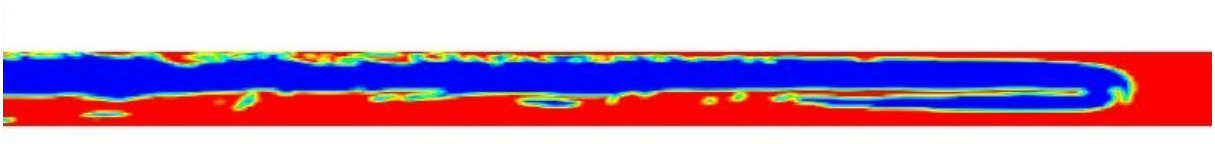

Figure 34 Whole pipe 7 cells/cm

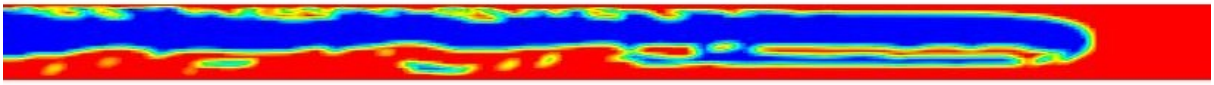

Figure 35 Whole pipe 4 cells/cm

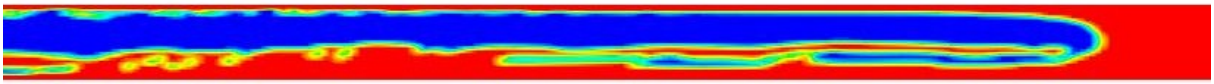

Figure 36 Half pipe 4 cells/cm

The 4 cells/cm mesh demanded almost 200 000 cells per meter pipe which and the improved accuracy of the 7 cells/cm and approximately 600 000 cells per meter pipe cannot be justified since it increases the computational cost by approximately a factor 5. Figure 37 show the mass fraction flowing through surfaces located after 1,2,3,4 and 5 meters into the pipe for the two different meshes.

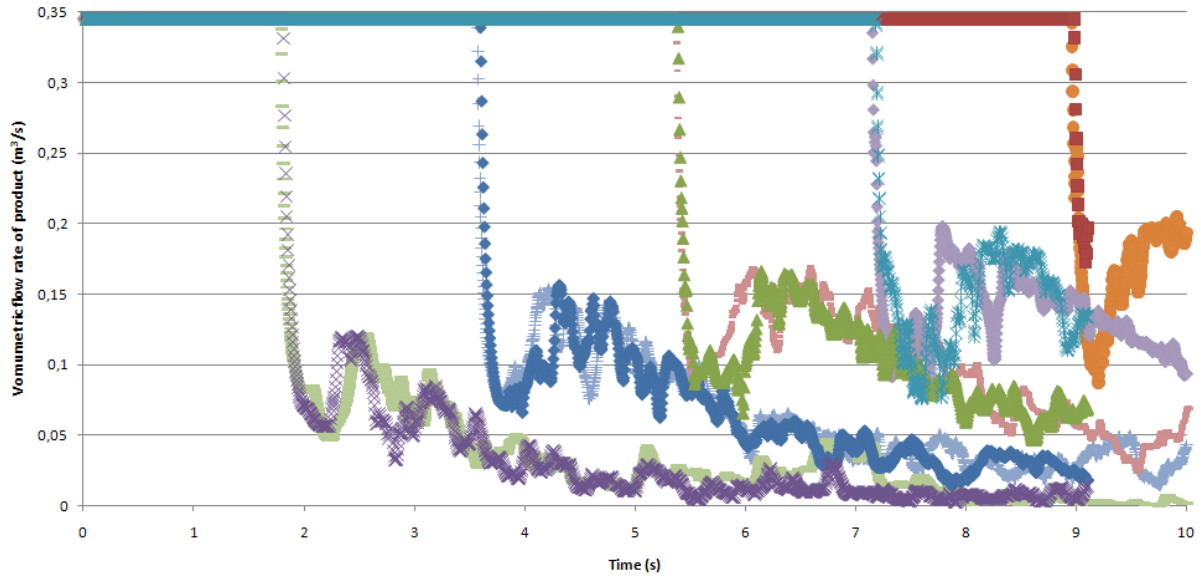

Figure 37 Comparison of the volumetric flow rate of product for 4 cells/cm and 7 cells/cm mesh

A comparison between the volumetric flow rate for the two meshes show an increasing difference in the flow between the two meshes. Up to about 3 meters down the coarse mesh follow the finer quite well but from the 4 meters measuring point and onwards the two curves have lost most resemblance putting the methods ability to capture the residual film into question. The breakthrough times for the two fluids remain similar indicating mesh independence for the breakthrough time has been achieved.

Symmetry

Concerns about using the symmetry in the pipe was investigate by doing similar simulations on a whole and a half version of the 4 cells/cm pipe seen in figure 35 and 36. Little gain in accuracy was seen from the simulations simulating the whole pipe instead of using the symmetry in the pipe and the added computational cost from simulating the whole pipe could preferably be used on improved flow resolution. All simulations presented in this paper are made on a whole pipe.

4.7 Time step size

The effect of various courant numbers was also investigated. The results from using a time step size of 0.005 seconds with courant numbers in the range 0.8-0.6 was compared to a time step size of 0.0025 seconds. The whole 5 meters of flow was simulated and both simulations had a brake through time of 8.95 seconds indicating no need for time steps smaller than courant number 1. Simulations of courant numbers larger than 1 caused increasing underestimations of the displacement efficiency.

4.8 VOF formulation

Various VOF formulations were tested to see how well they could capture the displacement process. Most of the VOF formulations resulted in an unacceptably high numerical diffusion between the phases and only two models created a fine interface, the Geometric reconstruction scheme and the CICSAM scheme. The CICSAM scheme were however unable to capture the instabilities at the mesh densities that were computationally affordable as can be seen in figure 38.

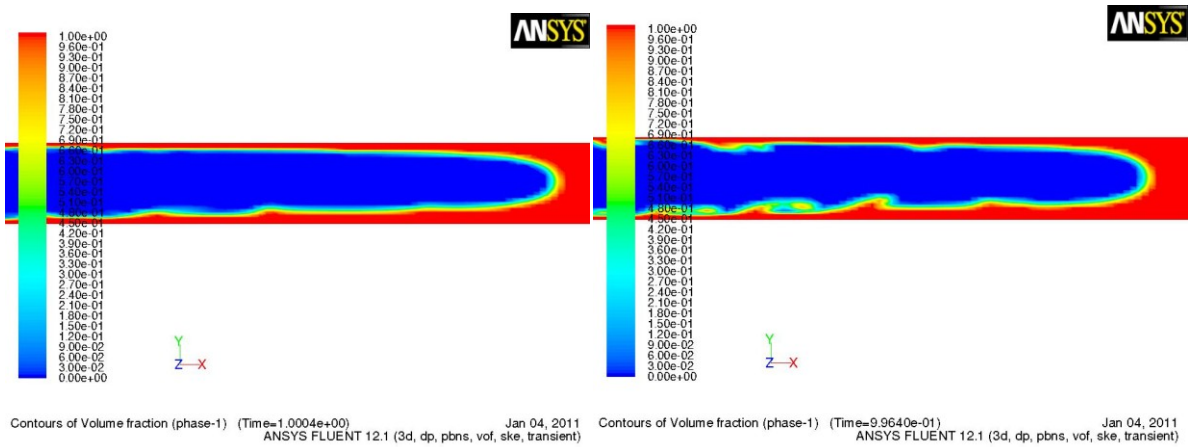

Figure 38 Comparison of CICSAM and VOF simulation to the left and geometric reconstruction to the right

4.9 Discretisation

Similar test were made on the discretization method where the momentum equation was discretized with both first order upwind and Quick. The instabilities present were noticeably damped when using the first order upwind method. Since there were no convergence issues

present when using the Quick discretization and it even showed a faster convergence than the upwind method there was no reasons not to use Quick.

4.10 Laminar axisymmetric simulations

Initial test of the CFD code was conducted by trying to recreate the Gabard and Hulins experiments on vertical displacement of Newtonian fluids in a 1 meter long and 0.024 meters in diameter pipe using CFD simulations [1]. The velocities used during the experiments were 0.002 – 0.02 m/s for viscosity ratio 85 and 350 and 0.002 m/s to 0.0005 m/s for viscosity ratio 6. Both fluids were Newtonian and had the same density.

The purpose of these simulations was to investigate how well the initial residual wall film thickness behind the front of the displacing fluid was predicted in a simple case.

The experiments showed no effect of velocity and the experimental and computed residual film thickness is listed in table 2.

	N=6	N=85	N=350
Experimentally obtained results:	29 %	38∓1 %	38∓1 %
Computed results:	30 %	35,5 %	36,3%

Table 2

The flow was assumed to be laminar and axisymmetric and mass transfer and surface tension was assumed to b nonexistent. The discretization used for the momentum equation was QUICK and the VOF formulation chosen was geometric-reconstruction.

The CFD simulations showed no effect of velocity on the residual film thickness in the ranges tested.

Various meshes was tested for grid independence which was achieved at 6 cells/cm for the N=85 and N=350 viscosity ratios. For the N=6 simulation a cell density of 12 cells/cm was required. The simulations showed good agreement with the experimental data for all viscosity ratios.

The displacement finger reached its final residual thickness after less than 0.1 meter for both the 85 and 350 viscosity ratio simulations. Upstream the residual films all exhibited instabilities.

Figure 39 Front for viscosity ratio 85

4.11 LES simulations

In order to gather understanding of the instabilities present in the flow and to understand what impact the poor turbulence modeling has on the simulation, the displacement process was simulated using LES turbulence model. Two cases on the standard and refined mesh were simulated to see if grid independence was achieved.

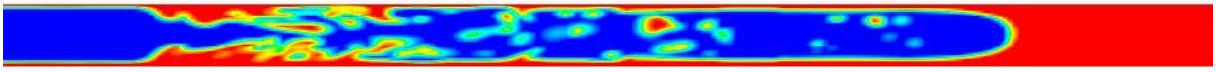

Figure 40 Displacement front after 3 seconds, LES simulation coarse mesh

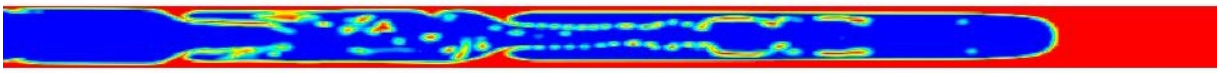

Figure 41 Displacement front after 3 seconds, LES simulation fine mesh

Comparisons of the results for the two meshes show that no mesh independence was achieved. The instabilities present in the two LES simulations after 3 seconds indicate that the instabilities present in the displacement process decreases with an increased cell density.

The displacement efficiencies of the two processes yield 0.59 for the coarse mesh and 0.57 for the fine mesh. This can be compared with the result 0.62 obtained from with the k-epsilon model.

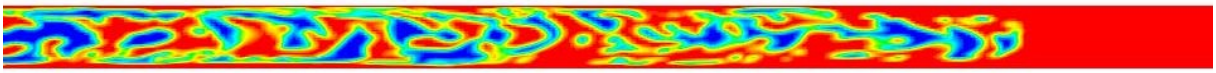

Figure 42 Coarse mesh after 8.6 seconds

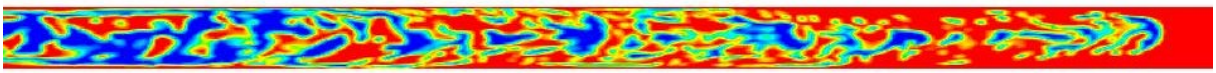

Figure 43 Fine mesh after 8.6 seconds

The LES simulations were considerably less stable than the k-epsilon simulations resulting in a complete collapse of the displacement profile into a mixed flow. Figure 42 and 43 show the fully mixed state arising during the displacement process after 8.6 seconds.

4.12 Conclusion

The finally chosen method is summarized in table 3 and 4 together with the boundary conditions used.

The case settings for the final method were:

VOF formulation:	Geometric reconstruction
Solver:	Pressure based
Pressure velocity coupling:	PISO
Gradient:	Least square based
Pressure:	PRESTO!
Momentum, turbulent kinetic energy, turbulent dissipation discretization:	QUICK
Time discretization:	First order explicit
Turbulence model:	k-epsilon
Mesh:	Full pipe, O-mesh, 4 cells/cm

Table 3

Boundary conditions:

	Inlet:	Outlet:	Wall:
Boundary condition:	Velocity inlet Velocity: parabolic profile UDF. Turbulence: 6.3 cm hydraulic diameter, 5 % turbulent intensity.	Outflow	Wall treatment for smooth walls, no slip and slip UDF.

Table 4

As an initial condition the entire pipe was filled with the product and patched with a power law velocity profile.

5. Results and discussion

5.1 Parameter study

Studies on what effect variations of the parameters of the displaced fluid had on the displacement efficiency were investigated using the method developed in section 4. The following parameters were investigated:

- Density difference
- Power law index
- Fluid consistency index
- Rheology model
- Yield stress
- Volumetric flow rate
- Slip

Gravitational effects

The gravitational effects have been investigated by simulating the first 5 meters of the displacement process of a power law fluid with gravitational effects included and excluded by adding a 32 kg/m^3 density difference between the fluids. A Herschel Bulkley fluid with density difference of 52 kg/m^3 was also displaced by water with gravitational effects included and excluded. A 32 kg/m^3 is an estimate of the density difference encountered when displacing common dairy products, a process which seldom encounters higher density differences than 60 kg/m^3.

K (Pa*s^n)	n (-)	Δρ (kg/m^3)	Q (l/s)	Breakthrough time (s)	Displacement time, 1-5 meter: (s)	Displacement efficiency (-)
5	0.35	0	1.08	8.95	7.15	0.62
5	0.35	32	1.08	8.97	7.15	0.62

K (Pa*s^n)	n (-)	Tao (Pa)	Slip (m/sPa)	Δρ (kg/m^3)	Q (l/s)	Breakthrough time (s)	Displacement time, 1-5 meter: (s)	Displacement efficiency (-)
4.5	0.5	8	0	0	1.08	8.59	6.86	0.59
4.5	0.5	8	0	52	1.08	8.53	6.87	0.59

The results indicate that the inclusion of gravitational effects has a little impact on the displacement process for density differences usually encountered in the food processing industry.

Figure 44 shows the results of a simulation of how the displacement front develops in time and compares the shape of the front after 3, 6 and 9 seconds. It can be seen that the front instantaneously becomes vertically displaced by the buoyancy forces. After an initial displacement it does however stabilize on a specific height and no further displacement takes place. It is thus likely that the absence of impact from gravity on the displacement efficiency is valid throughout the entire pipe system.

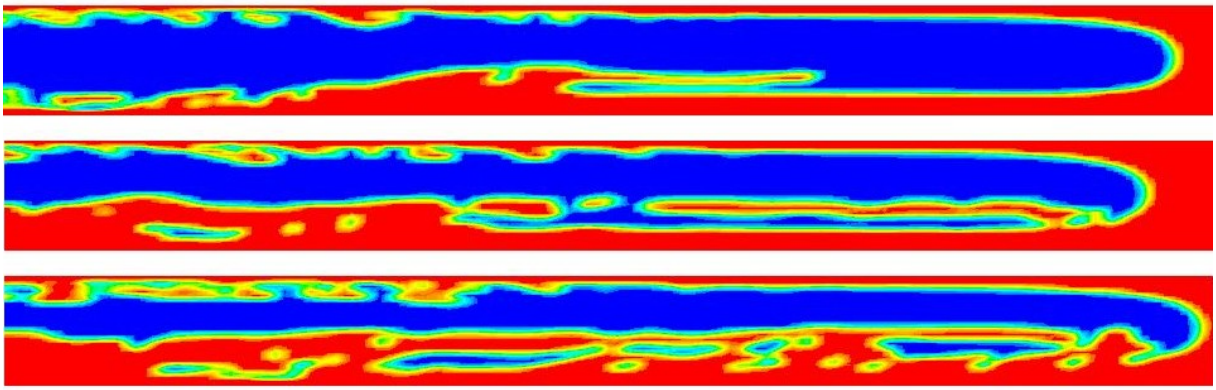

Figure 44 Comparison of the displacement front after 3 s top figure, 6 s middle figure and 9 s bottom figure

Rheological effect on the displacement efficiency

Power law fluid

The displacement process for a power law fluid was simulated for various consistency indexes K and power law indexes n.

First the effect from variations on the fluids consistency index was tested.

K ($Pa*s^n$)	n (-)	Tao (Pa)	Slip (m/sPa)	Δρ (kg/m^3)	Q (l/s)	Breakthrough time (s)	Displacement time, 1-5 meter: (s)	Displacement efficiency (-)
10	0.35	0	0	40	1.08	8.64	6.90	0.60
5	0.35	0	0	40	1.08	8.97	7.15	0.62
2.5	0.35	0	0	40	1.08	9.25	7.36	0.63

A two fold increase or decrease of the apparent viscosity ratio between the two fluids has a small effect on the displacement efficiency. This indicates that the rheological data of the displaced product is not very sensitive to a low accuracy estimation of the fluid consistency or thixotropic effects. The difference is assumed to be related to an increasing and decreasing viscosity ratio between the fluids. It is then clear that the increased viscosity effect from the water-dissolved displaced product mixture has a small impact on the displacement efficiency and the decision to ignore any such effect was correct.

Vector graphs scaled with a reduction of the velocity of the displacement front for can be seen in figures 47 and 48 for the K=2.5 and K=10 cases. It is clear that an increase of the fluid consistency index has a large impact on the flow around the displacement front which becomes thicker when the consistency index increases. Not clear in these figures is that the velocity of the displaced fluid surrounding the displacing front decreases significantly more for higher consistency index fluids causing a lower displacement efficiency.

Also variations of the power law index was simulated

K ($Pa*s^n$)	n (-)	Tao (Pa)	Slip (m/sPa)	Δρ (kg/m^3)	Q (l/s)	Breakthrough time (s)	Displacement time, 1-5 meter: (s)	Displacement efficiency (-)
5	0.45	0	0	40	1.08	8.39	6.69	0.58
5	0.35	0	0	40	1.08	8.97	7.15	0.62
5	0.25	0	0	40	1.08	9.76	7.78	0.67

Now a considerably bigger effect is seen. This is most likely related to a decrease in the maximum velocity with increasing shear thinning behavior. An accurate estimation of the power law index is thus important and Thixotropic effects on the power lay index can noticeably influence the displacement process.

Herschel Bulkley fluid

The effects from varying the parameters of the Herschel-Bulkley fluid during displacement were also tested.

K ($Pa*s^n$)	n (-)	Tao (Pa)	Q (l/s)	Breakthrough time (s)	Displacement time, 1-5 meter: (s)	Displacement efficiency (-)	Unyielded radius (m)
2.5	0.35	8	1.08	10.49	8.38	0.72	0.016
2.5	0.35	4	1.08	9.97	7.95	0.68	0.013
2.5	0.35	0	1.08	9.23	7.33	0.63	0

K ($Pa*s^n$)	n (-)	Tao (Pa)	Q (l/s)	Breakthrough time (s)	Displacement time, 1-5 meter: (s)	Displacement efficiency (-)	Unyielded radius (m)
4.5	0.5	8	1.08	8.59	6.86	0.59	0.085
5	0.45	0	1.08	8.38	6.69	0.58	0

The displacement efficiency reduction experienced when introducing a yield stress on the displaced fluid reduces with increased fluid viscosity. This is to be expected because a decrease in size of the unyielded cylinder in the centre of the flow as the fluid becomes more viscous and the shear stresses increase.

Velocity vector graphs with superimposed phase profiles which are scaled to display the difference from the steady state displacement front velocity for 8 Pa, 4 Pa and no yield stress fluids are shown in figures 45, 46 and 47. They illustrate the effect yield stress has on the displacement front thickness which largely determines the displacement efficiency.

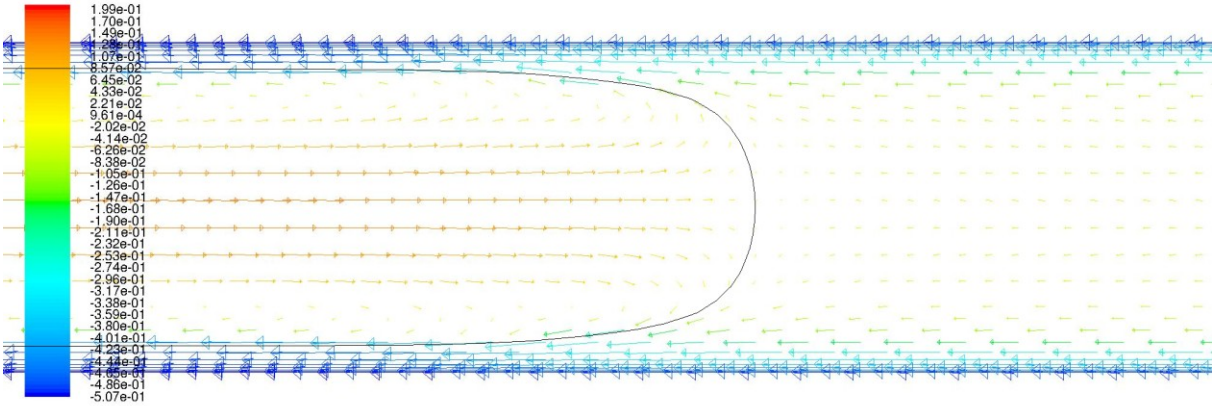

Figure 45 Scaled vector graph for K=2.5, n=0.35, τ=8, black line indicate fluid-fluid interface

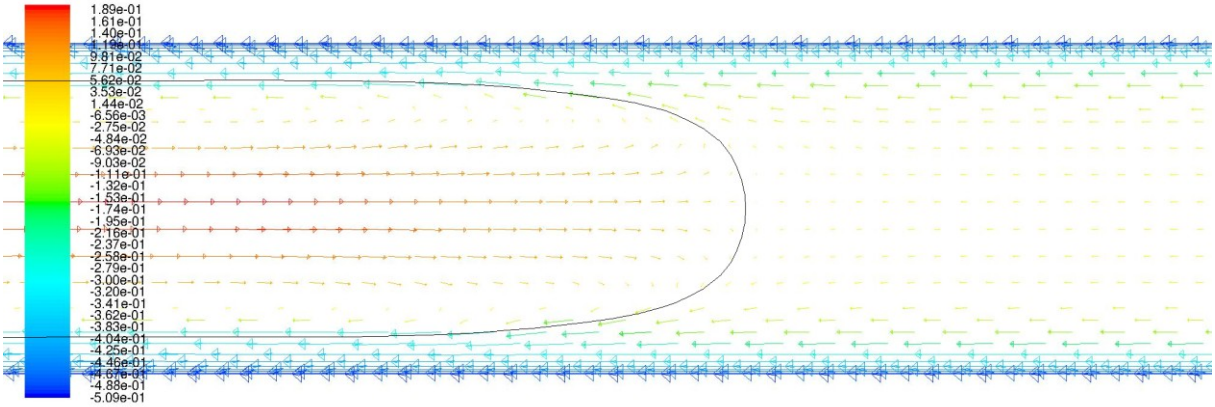

Figure 46 Scaled vector graph for K=2.5, n=0.35, τ=4, black line indicate fluid-fluid interface

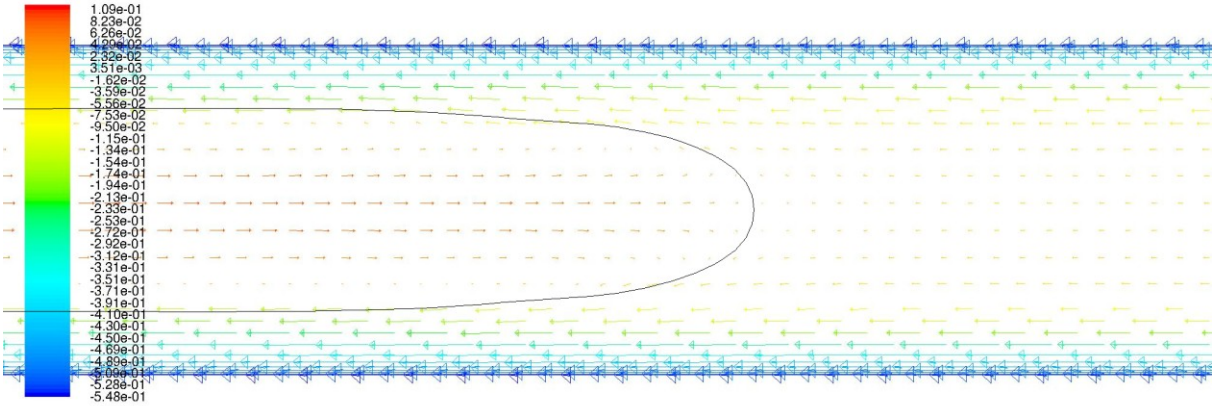

Figure 47 Scaled vector graph for K=2.5, n=0.35, τ=0, black line indicate fluid-fluid interface

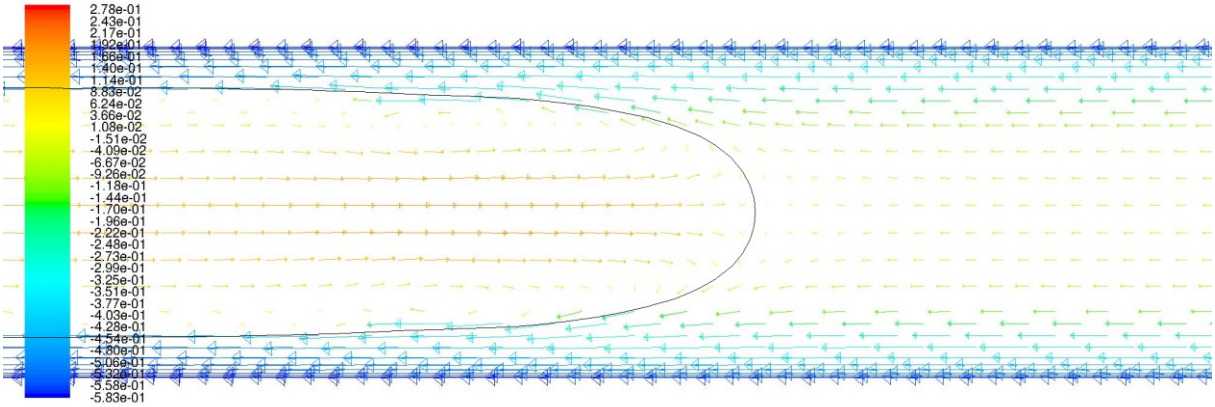

Figure 48 Scaled vector graph for K=10, n=0.35, τ=0, black line indicate fluid-fluid interface

5.2 Volumetric flow rate

Variations of the volumetric flow rate were also tested indicating that the displacement efficiency decreases with a decrease in flow rate. This is most likely due to an increased apparent viscosity caused by decreasing shear rates in a shear thinning fluid modelled by the power law $\mu = K * (\dot{\gamma})^{n-1}$.

This was also valid for the yield stress fluid which according to experiments [1] should have a contrary reaction to a decrease in flow rate. A theory to why this happened is that the yield stress was too low to have a large impact on the displacement process which can be seen in figure 53 where power law modelling and Herschel Bulkley modelling is compared indicating that the unyielded cylinder in the centre of the displaced fluid is too small to have a large impact. The increased apparent viscosity then had a larger impact on the displacement velocity causing the displacement efficiency to decrease.

An increasing displacement efficiency with increasing flow rate was also seen in the measurements made at Tetra Pak which showed an increased efficiency with flow rate for all four cases.

K (Pa*s^n)	n (-)	Tao (Pa)	Slip (m/sPa)	Δρ (kg/m^3)	Q (l/s)	Breakthrough time (s)	Displacement time, 1-5 meter: (s)	Displacement efficiency (-)
5	0.35	0	0	40	0.57	15,85	12.7	0.58
5	0.35	0	0	40	1.08	8.97	7.15	0.62
2.5	0.35	0	0	40	0.57	16,53	13.2	0.61
2.5	0.35	0	0	40	1.08	9.25	7.36	0.63
4.5	0.5	8	0	0	0.57	15.75	12.6	0.58
4.5	0.5	8	0	0	1.08	8.59	6.86	0.59

5.3 Slip

The effects of slip between the fluid and the wall were also simulated for yield and non yield stress fluids. Because the slip condition causes the displaced phase to slide along the walls it naturally has a displacement efficiency increasing effect. The slip condition caused an increase in displacement efficiency for both cases but the effect was twice as big for the yield stress fluid. This is likely due to the fact that for yield stress fluids the slip also decreases the shear stress in the displaced fluid increasing the diameter of the unyielded cylinder in the centre of the pipe.

K (Pa*s^n)	n (-)	Tao (Pa)	Slip (m/sPa)	Δρ (kg/m^3)	Q (l/s)	Breakthrough time (s)	Displacement time, 1-5 meter: (s)	Displacement efficiency (-)
5	0.35	0	0.0024	0	1.08	9.4	7.52	0.65
5	0.35	0	0	0	1.08	8.95	7.15	0.62
4.5	0.5	8	0.0024	0	1.08	9.44	7.57	0.65
4.5	0.5	8	0	0	1.08	8.59	6.86	0.59

5.4 Comparison between calculated displacement velocity and the velocity profile of the displaced fluid.

A theory on how to predict the displacement velocity is to use the maximum velocity of the displaced profile calculated from eq. 3-4 and eq. 3-8. To evaluate this theory, comparisons

between the maximum velocity and the displacement velocity have been made. The displacement velocity has been compared with the maximum velocity in the fully developed simulated flow and an overestimation factor has been calculated as the difference between the two velocities divided by the maximum velocity.

For the high velocity case of the displacement of a power law modeled fluid with power law index 0.35 for various consistency indexes a large difference overestimation can be seen in table 6. Increasing the consistency index results in an increased overestimation. In table 7 the overestimation factor is compared for fluids with the same consistency index but with different power law indexes is compared. It appears that the power law index has a small influence on the overestimation factor and the consistency index is the determining parameter.

K ($Pa*s^n$)	n (-)	Q (l/s)	Displacement efficiency CFD (-)	Displacement efficiency maximum velocity (-)	Overestimation factor (-)
10	0.35	1.08	0.6	0.66	0.1148
5	0.35	1.08	0.62	0.66	0.0758
2.5	0.35	1.08	0.63	0.66	0.0451

Table 6

K ($Pa*s^n$)	n (-)	Q (l/s)	Displacement efficiency CFD (-)	Displacement efficiency maximum velocity (-)	Overestimation factor (-)
5	0.45	1.08	0.58	0.62	0.0753
5	0.35	1.08	0.62	0.66	0.0758
5	0.25	1.08	0.67	0.72	0.0756

Table 7

Comparisons between the overestimation factors for the two different volumetric flow rates shown in table 8 indicate an increased overestimation with decreasing flow rate.

K ($Pa*s^n$)	n (-)	Q (l/s)	Displacement efficiency CFD (-)	Displacement efficiency maximum velocity (-)	Overestimation factor (-)
5	0.35	0.57	0.58	0.66	0.141
2.5	0.35	0.57	0.61	0.66	0.0979
5	0.35	1.08	0.62	0.66	0.0758
2.5	0.35	1.08	0.63	0.66	0.0451

Table 8

The underestimation factor has also been calculated for Herschel-Bulkley fluids and for slip flows ad are shown in table 9. The modeling of a fluid as a Herschel Bulkley fluid increased the underestimation factor. The simulation of slip had opposing effects on Power law and Herschel-Bulkley modeled fluids with an underestimation decreasing effect on the Power law modeled fluids and an increasing effect on the Herschel-Bulkley fluids.

K ($Pa*s^n$)	n (-)	Q (l/s)	Tao (Pa)	Slip (m/sPa)	Displacement efficiency CFD (-)	Displacement efficiency maximum velocity (-)	Overestimation factor (-)
4.5	0.5	1.08	8	0	0.59	0.66	0.1148
2.5	0.35	1.08	8	0	0.72	0.78	0.0774
4.5	0.5	1.08	8	0.0024	0.65	0.73	0.1218
5	0.35	1.08	0	0.0024	0.65	0.70	0.0724

Table 9

A comparison between underestimation factor and consistency index for the various cases can be seen in figure 49.

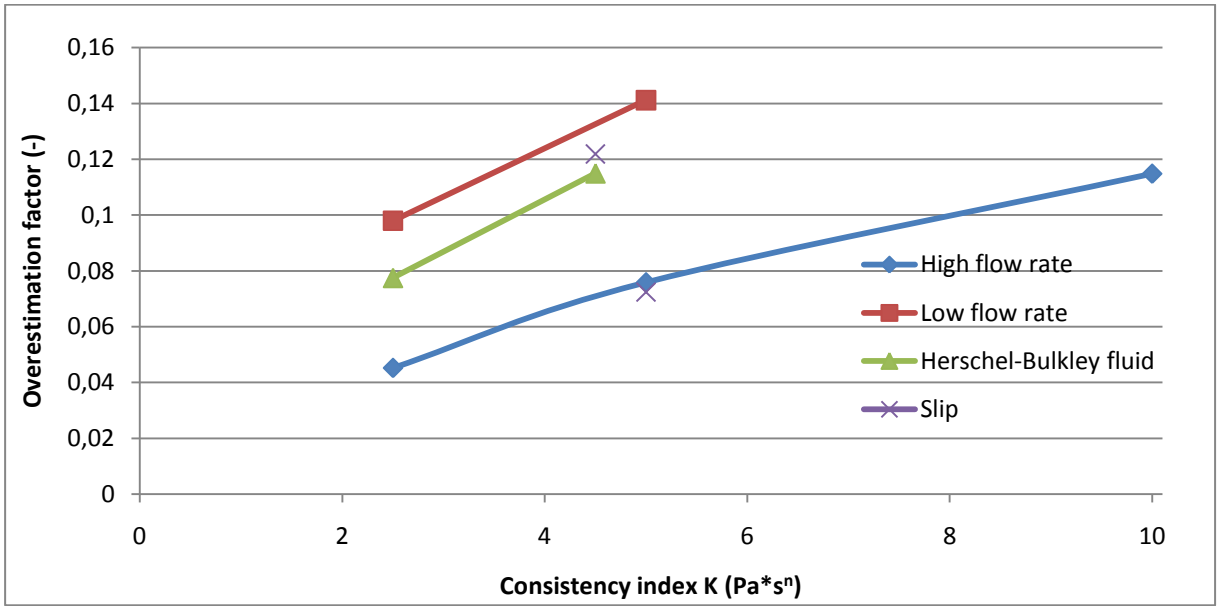

Figure 49 Variation of underestimation factor with consistency index for various cases

5.5 Experiments

In 2001 Tetra Pak conducted a series of experiments on the breakthrough time and phase distribution during fluid displacement in pipe systems. Measurements were made for 8 different cases for 2 different pipe systems. At the outlet of the system the mixture was collected approximately every 5 seconds and the mixture was analysed for the total solid content.

Both systems consisted of both pipe sections and various other components which were not taken into account when calculating the total volume. System 1 was approximately half the size of system 2.

The 8 cases for the 2 systems consisted of water-product 1, product 1-water, product 2 -water and water-product 2 displacement for 2 different volumetric flow rates, 0.000578-0.00569 m^3/s and 0.001072 m^3/s.

As a comparison of the experimentally obtained breakthrough times and the breakthrough time of a perfect plug flow has been computed. The experimental breakthrough time is taken at the time when the total solids content in the outlet starts to sink and is thus delayed with up to 5 seconds. The reported experimental values are taken as the average for all the simulations of that case.

	Experimental/Plug flow ratio:
High flow, system 2, product 1	0,89
High flow, system 1, product 1	0,94
Low flow, system 2, product 1	0,72
Low flow, system 1, product 1	0,74
High flow, system 2, product 2	0,60
High flow, system 1, product 2	0,67
Low flow, system 2, product 2	0,55
Low flow, system 1, product 2	0,66

5.6 Analysis of experimental data

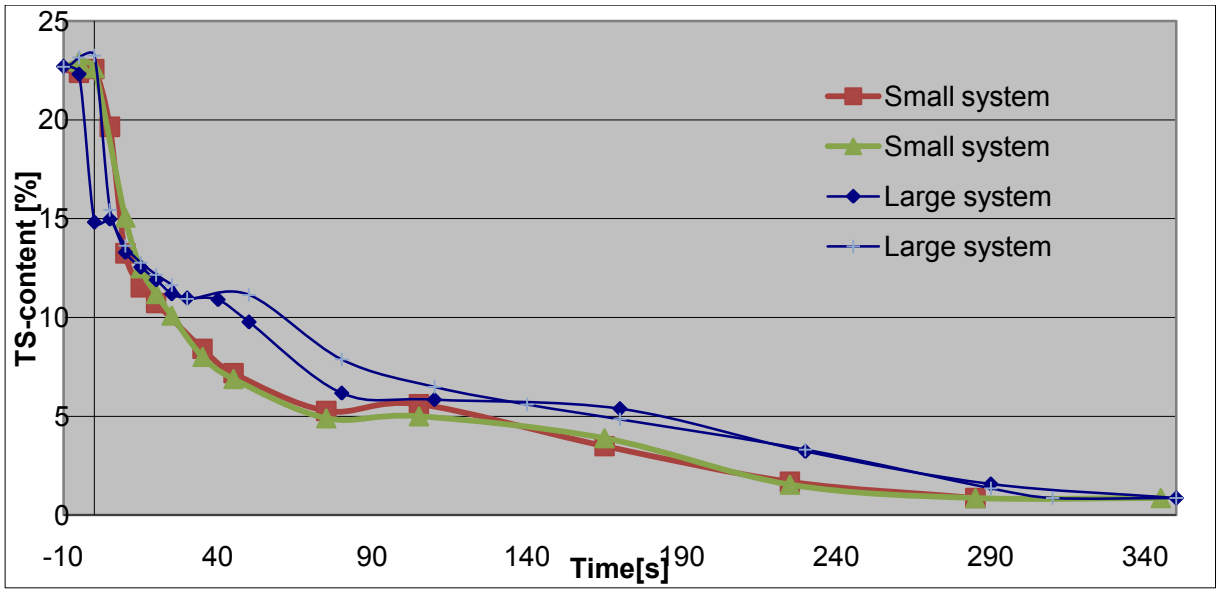

Figure 50 High mass flow rate displacement of product 2 data in the large and the small system, where plotted time stars at the time of the breakthrough

The efficiency of the displacement process of product 2 by water varies in the range of 0.56 – 0.7 and decreases with an increasing pipe system length which is most likely caused by the difference in system volumes between the large and the small systems. This is caused by the volume of the pump, filter, bends and valves not taken into account. This results in a relatively smaller underestimation of the volume in the large system which causes less overestimated displacement efficiencies.

The experimental data of the residual film obtained from the high flow rate displacement experiments of product 2 was compared for the large and small displacement systems by using no scaling and only comparing the outflow of the systems after the breakthrough time in the outlet.

This way a comparison between the two residual films can be made without any scaling effects on the residual films. The result is shown in figure 50 and a clear similarity can be seen. The obvious difference being that the film is thicker in the large pipe system. This indicate that a near steady state solution has been achieved for the residual film which require mass transfer or instabilities that remove product 2 from the residual film and mixes it with the water phase of the flow. An increased volume fraction for the displaced fluid for the large pipe system is then unavoidable as the water phase becomes mixed up with product 2. As the residual film erodes or becomes removed by instabilities or flow vertices it will end up being transported by the water velocity field. Because this flow has a maximum velocity approximately 20 % higher than the mean velocity it can impossibly be removed as quickly as the displacement front which can be almost twice the mean velocity. This means that a steady state displacement is impossible. In figure 50 it can be noted that the removal of the final residual film took approximately 50 seconds longer in the large system.

An estimation of the product volume in the residual film at breakthrough time is 71 liters for the large system. For the small system the corresponding value was 45 liters.

Comparisons to the behaviour of the residual film for the low velocity case in figure 52 imply a drastically different behaviour for the low mass flow rate case. Figure 52 is scaled against breakthrough time which is assumed to vary linearly with the system volume. In the low mass flow rate case the residual film seems to scale with pipe system size and thus grow linearly with pipe length. This indicates an absence of mass transfer mechanism in the displacement process.

This behaviour of the residual film can be explained as a result of an erosion dominated mass transfer mechanism which is activated at a critical shear rate leading to no or a very limited mass transfer rate in the low flow rate case. Because it takes more than 300 seconds for the mass transfer process to erode the residual film, the erosion must be very slow and can be ignored in our simulations of a 5 meter long pipe.

In the case of the displacement of product 1 a similar behaviour can be seen at low flow rate where the volume fraction profiles are similar when scaled for the large and small pipes as can be seen in figure 54. There are still large differences between the curves but this is most likely caused by inaccuracies during the experiments and possible standard variations of the displacement process.

The displacement profiles for high flow rate displacement of product 1 indicate that the process is considerably more complicated than the product 2 case. During the displacement in the short pipe system the profile appear almost plug like. A comparison with the longer pipe system indicates that it keeps its plug like displacement process but with a larger mixing zone making the displacement curve less flat.

This must be caused by a very high mass transfer mechanism. There are three theories to how this happens. The first possible explanation is that the product 1 is turbulent which results in a very large mass transfer from turbulent diffusion. The power law Reynolds number is calculated with equation 2 to 89 which indicates no turbulence in the product 1 phase which would be a requirement for turbulent diffusion which would increase the diffusion considerably. This is however very uncertain as little is known about turbulence in non-Newtonian fluids and the rheological data estimation is of low accuracy.

The second possible explanation is that the shear stress in the flow has reached a threshold value starting an erosion process of the product 1 into the water.

A third explanation is that the velocity is to high for the displacement to remain stable and a breakdown of the displacement front takes place, this combined with diffusion creates a plug like displacement.

From the data for product 2 displacing water shown in figure 56 it is clear that there is a high displacement efficiency for the case of a low viscosity fluid being displaced by a more viscous one, as can easily be showed by numerical simulations. The displacement front is showed in figure 51.

Figure 51 Product 2 displacing water, front after 3 seconds of displacement

5.7 Verification

When comparing the displacement velocity for various fluids it can be seen that the displacement front reaches a steady state velocity after less than 1 meter. An example is the K=5, n=0.35, Q= 1.08 l/s case for which the displacement front velocity for the distance 1-2, 2-3, 3-4 and 4-5 meters down the pipe is computed and tabulated in table 1.

Pipe region	1-2 meters	2-3 meters	3-4 meters	4-5 meters
Displacement time	1.79 s	1.79 s	1.78 s	1.79 s

Table 5

The time it took the displacement front to travel 1 meter was thus between 1.78 and 1.79 seconds and it can be considered to have reached a steady state.

The method chosen for comparison of simulated data to experimental data is therefore to calculate the time it takes the displacement front to travel from 1 to 5 meters downstream of the pipe and compare it to the displacement time for a perfect plug listed below. Only flow in the main pipe diameter of 6.3 cm has been simulated.

4 meter displacement time for plug at 0.001072 m^3/s: 11.6 s
4 meter displacement time for plug at 0.000578 m^3/s: 21.7 s

The results from the experiments was attempted to be recreated by simulations of the displacement process in a straight pipe where unknown factors such as pumps, valves and bends were ignored. The displacement was assumed to be fully developed after 1 meter and no slip or mass transfer was taken into account. First simulations of the displacement of product 2 by water were run for the power law and the Herschel Bulkley modeled Product 2.

In the simulations in this paper I will investigate the flow in the 6.3 cm in diameter pipe where it had a mean velocity:

High flow (0.001072 m^3/s) 0.3440 m/s

Low flow (0.000578 m^3/s) 0.1827 m/s

Water displacing product 2

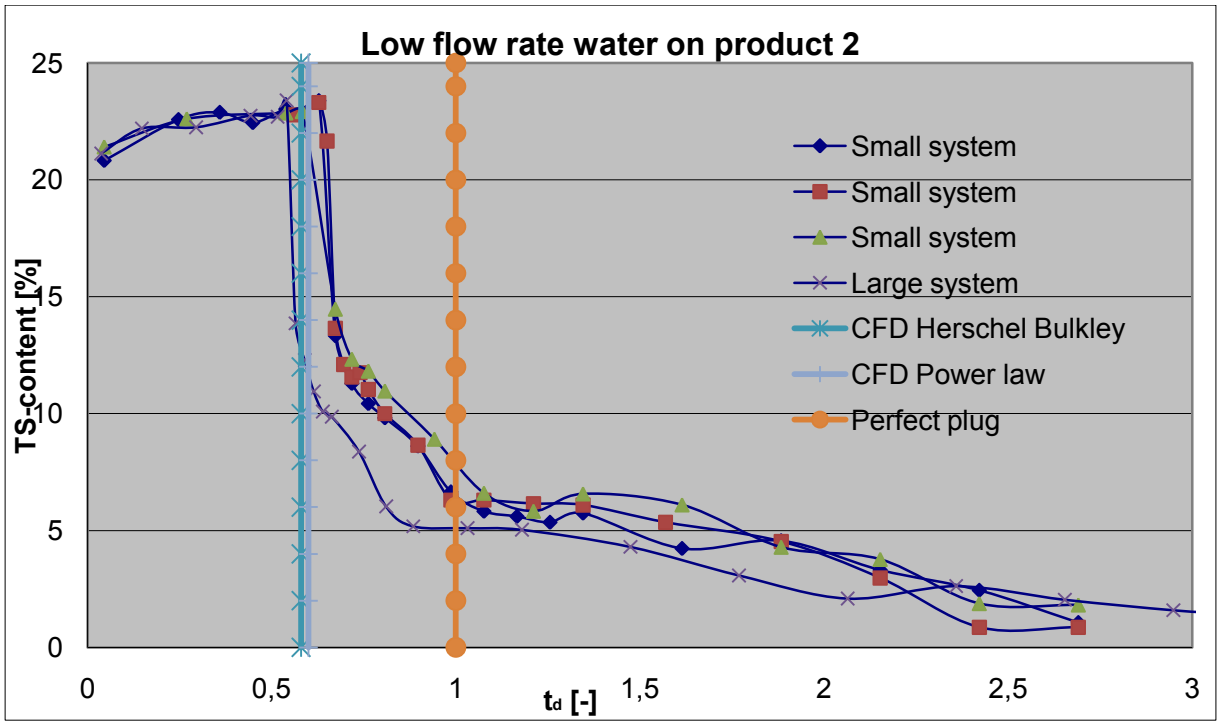

Figure 52 Scaled comparison between experimental data and simulated breakthrough time for product 2 at low flow rate

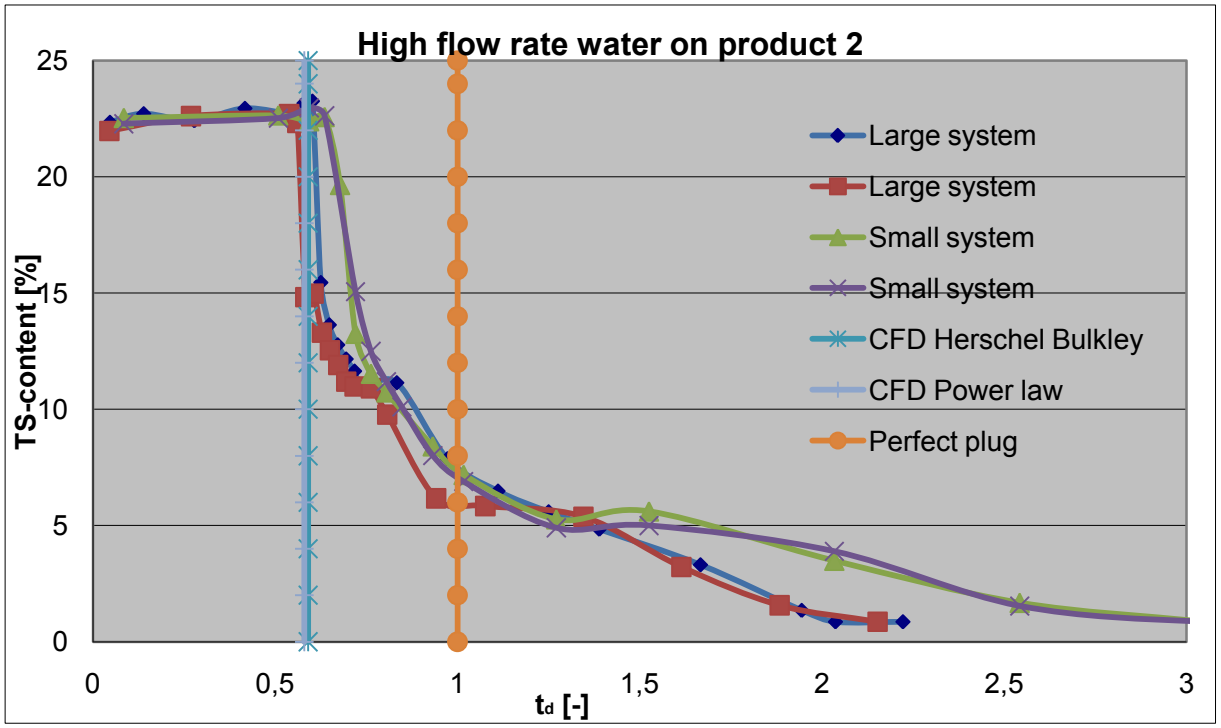

Figure 53 Scaled comparison between experimental data and simulated breakthrough time for product 2 at high flow rate

The displacement efficiencies for product 2 calculated for the two viscosity models for the two different volumetric flow rates is compared to a plug and experimental data scaled to the plug displacement time in figures 52 and 53. All four simulations display good results and are all within the spreading range of the experimental data.

Method	Experiment large system:	Experiment small system:	CFD Power law:	CFD Herschel-Bulkley:	Maximum velocity Power law:	Maximum velocity Herschel Bulkley:
Displacement efficiency high flow rate (-):	0.6	0.67	0.6	0.59	0.64	0.66
Displacement efficiency low flow rate (-):	0.55	0.66		0.58	0.64	0.64

Water displacing product 1

Further verification of the model was performed on the displacement of product 1 by water at high and low flow rates. The product 1 was like the product 2 modelled both as a power law fluid and a Herschel Bulkley fluid.

For the low flow rate case the breakthrough time in the experimental data was speared out in a large range making comparison it hard to compare them with the simulations. The Herschel Bulkley simulation gave good results while the power law result was unsatisfactory as showed in figure 54.

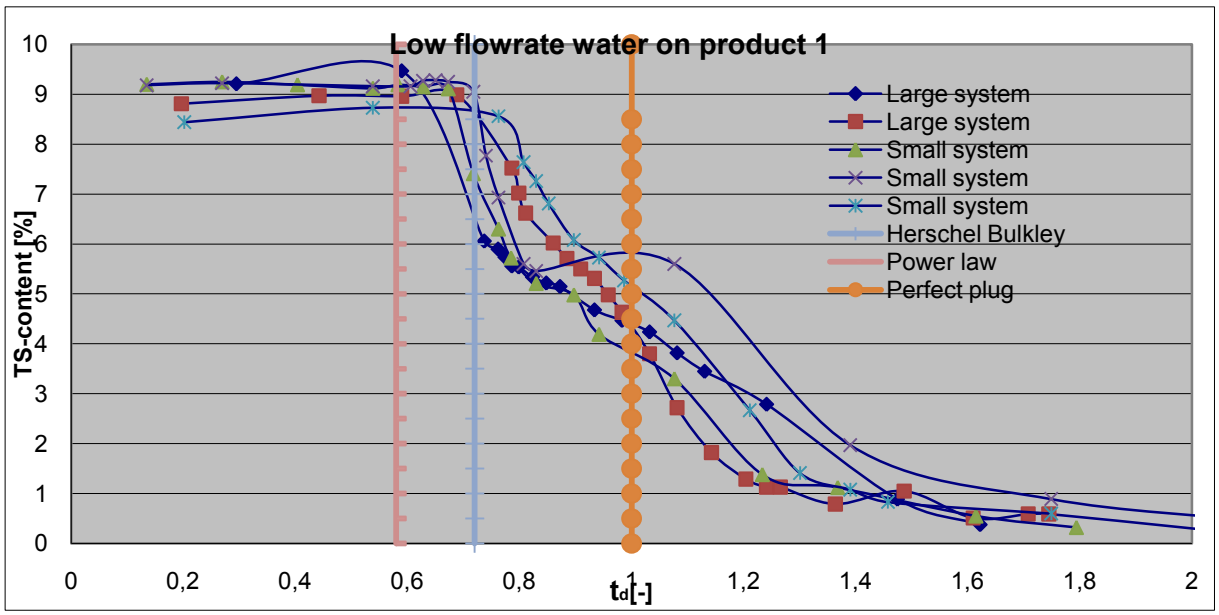

Figure 54 Scaled comparison between experimental data and simulated breakthrough time for product 1 at low flow rate

For the high flow rate case the results showed very poor agreement with the experiments. None of the models managed to capture the plug like displacement. The poor agreement to the experimental results is likely to be caused by not modeling the turbulence in the product 1 phase or any mass transfer between phases.

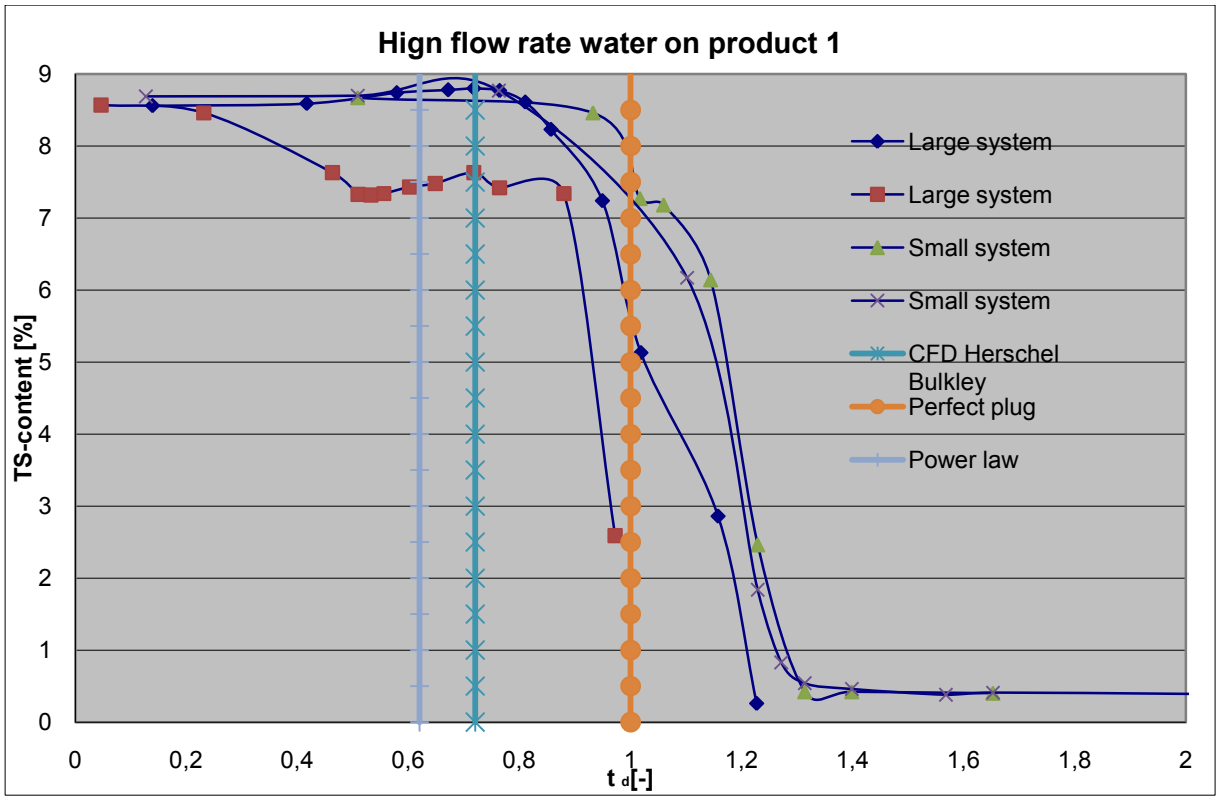

Figure 55 Scaled comparison between experimental data and simulated breakthrough time for product 1 at high flow rate

Method	Experiment large system:	Experiment small system:	CFD Power law:	CFD Herschel-Bulkley:	Maximum velocity Power law:	Maximum velocity Herschel Bulkley:
Displacement efficiency high flow rate (-):	0.89	0.94	0.62	0.72	0.67	0.778
Displacement efficiency low flow rate (-):	0.72	0.74	0.58	-	0.67	-

Displacing water by product 1

The high flow rate displacement of water by product 1 was also simulated where the product 1 was modeled as a power law fluid. A plug like displacement took place with only a thin product 1m of water surrounding the product 1. The simulations instantaneously reached a steady state and only the first 3 meters of flow was simulated. The displacement efficiency has been plotted together with scaled experimental data for high and low flow rates in figure 56 and 57 and show good agreement. This was expected since there are few complications like troublesome turbulence modeling, instabilities or possible mass transfer present in such a plug like displacement.

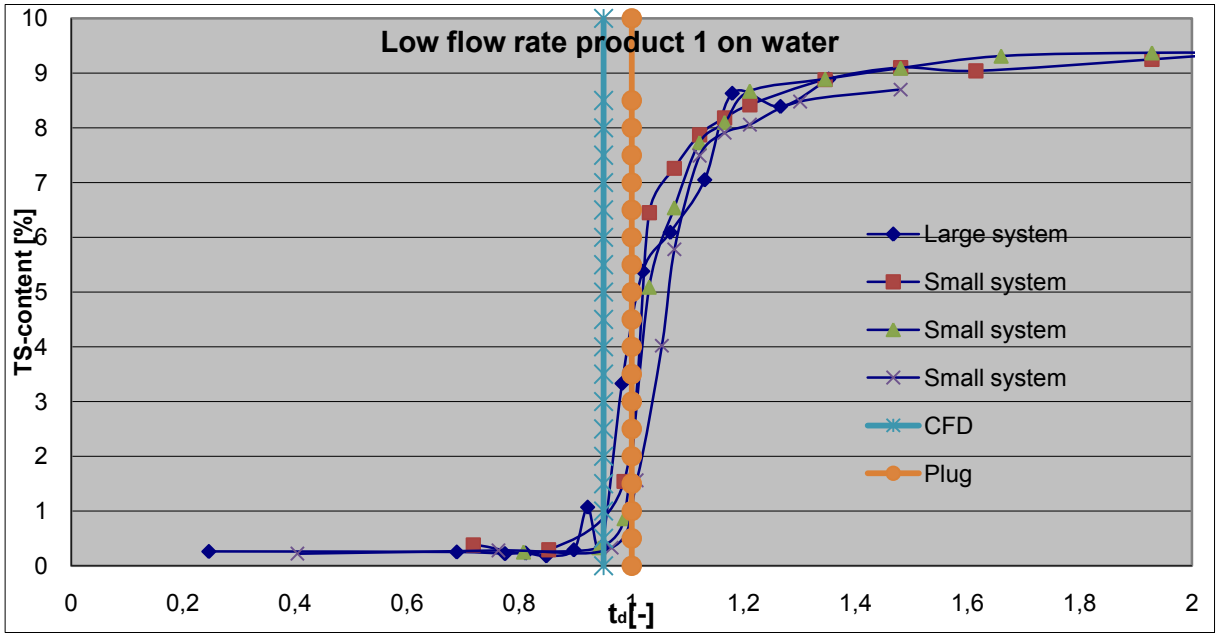

Figure 56 Scaled comparison between experimental data and simulated breakthrough time for product 2 displacing water at low flow rate

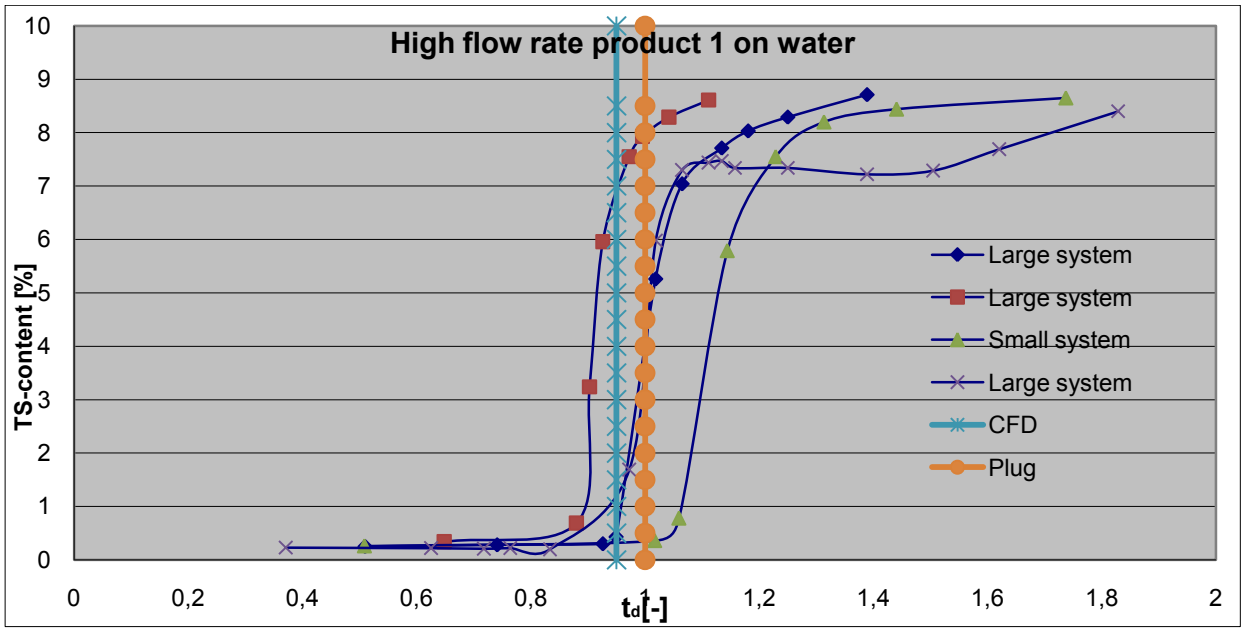

Figure 57 Scaled comparison between experimental data and simulated breakthrough time for product 2 displacing water at low flow rate

Comparison between experimental, simulated and maximum velocity values for the two cases is compared in table 10.

Method	Experiment:	CFD:	Maximum velocity:
Displacement efficiency high flow rate (-):	0.95	0.95	0.82
Displacement efficiency low flow rate (-):	0.98	-	0.82

Table 10

5.8 Long pipe simulation

The displacement of product 2 was also simulated in a longer pipe to see how well it could predict the outflow of the residual film after breakthrough.

The high flow rate displacement of a Herschel Bulkley modeled product 2 was simulated in a 20 meter long 6.3 cm in diameter pipe. The volumetric outflow of the product after 5, 10, 15 and 20 meters was averaged over the last second and scaled against the displacement time of a perfect plug and compared to experimental data in the large and small displacement system in figure 58. It is clear that the model largely underestimates the residual film. The variations of the also averaged over the last two and a half seconds, unscaled residual film after various surfaces downstream the pipe was also compared in figure 59 where time 0 s was set as the breakthrough time at the various surfaces. It can be seen that the residual film is constantly growing as it flows downstream but when compared to the scaled results in figure 58 it is clear that the results are quite similar and not likely to be approaching the experimental results had simulations been run for a longer pipe.

The differences between the experimental and simulated results are possibly due to poor rheological modeling and effects such as slip. Other possible reasons might be absence of mass transfer in the simulations which would increase the flow rate of the product in the outlet by letting the dissolved product flow out with the water.

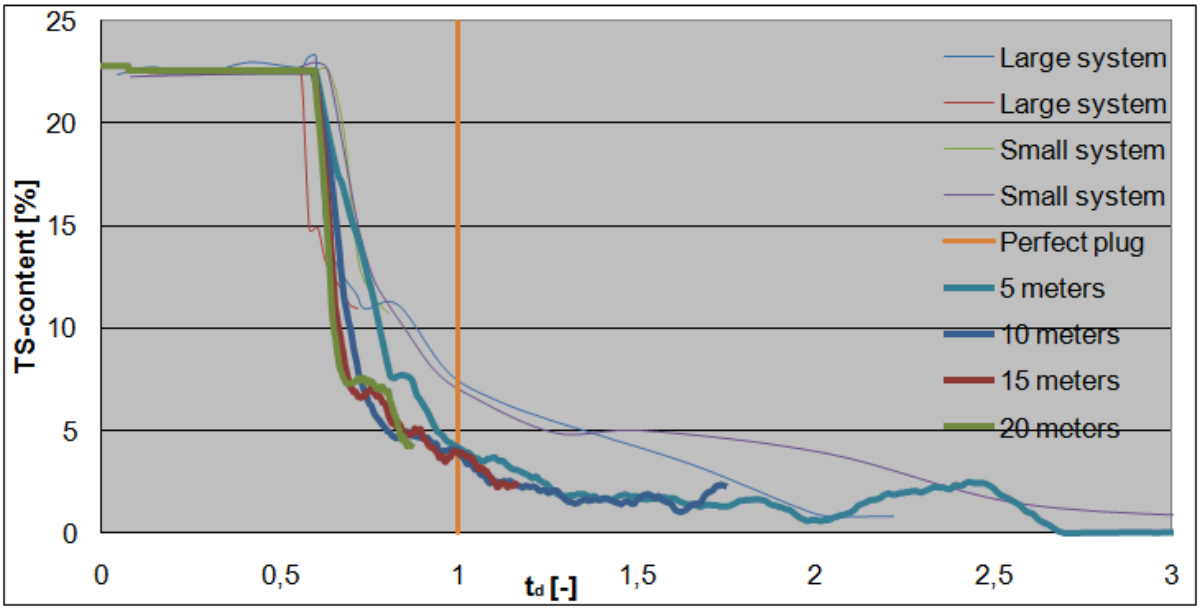

Figure 58 Simulated data of high flow rate displacement of product 2 compared to experimental data

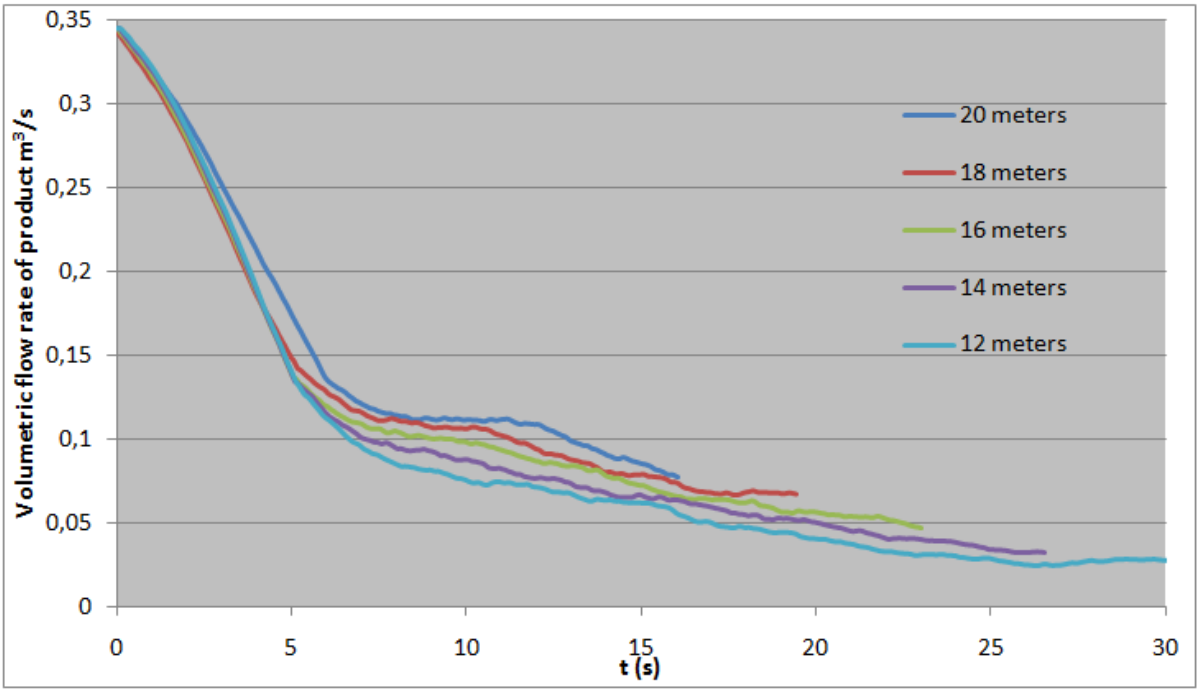

Figure 59 Simulated outflow rates of product 2 at various surfaces downstream, breakthrough time is set to 0 s for each surface.

6. Conclusion

A Volume of Fluid based method with no mass transfer taken into account was chosen to predict the displacement of a product by water. Problems concerning the stability of the displacement profile and diffusion between the two fluids make the method unsuitable for modeling large and complex systems. Modifications of the simulation to counteract instabilities and removal of diffused fluid to keep the interface sharp can be applied.

Two Large Eddy Simulations were run to verify the existence and ability of the method to capture the instabilities which may be present in the flow but was never verified as grid independent. The result from the LES simulations indicated a very unstable behaviour of the displacement process largely lost in the RANS simulations putting the ability of the code to capture the residual film into question.

The method was used to study the sensitivity to parameter variations in the displacement process. The displacement efficiency was shown to be very sensitive to parameters determining the velocity profile like power law index, yield stress and wall slip. The results were thus sensitive to choice of rheological model.

Variations in the consistency index had a smaller but also significant effect on the displacement. Variations of the density difference between the fluids, seemed to have a negligible impact on the displacement efficiency.

The three most important parameters determining the displacement efficiency were:

- Shear thinning index
- Yield stress
- Flow velocity

When attempting to verify the method by simulating a number of simplify cases of experiments, the VOF based CFD method accurately predicted the breakthrough time of the displacement process for most cases. Problems estimating deviant behaviour of the fluids still remain causing some simulations to differ greatly from the experiments. Factors such as turbulence in non-Newtonian fluids may cause unpredictable and considerable departures from the calculated values. Problems also arose when attempting to estimate the wall film residuals and the outflow of the product after breakthrough.

Further issues concerning the determination of important flow characteristics such as yield stress and slip reduces the confidence in estimated displacement efficiencies.

The most important factor determining the displacement efficiency appears to be the maximum velocity of the displaced fluid. Variations between the maximum velocity and the displacement velocity are determined by the flow in the proximity of the displacement front.

The interaction between the two fluids in the front of the finger where the displaced fluid is redirected around the displacing fluid determines the thickness of the initial residual film. This film might later become unstable and may be reduced due to mass transfer. The

simulations showed that the displacement front quickly developed a steady state and seemed unaffected by what was happening downstream.

7. References

[1] Gabard, C, Hulin, J, W, Miscible displacement of non-Newtonian fluids in a vertical tube, Eur. Phys. J. E 11, 231–241 (2003)

[2] Taylor, G, Dispersion of Soluble Matter in Solvent Flowing slowly through a tube, Proceedings of the Royal Society of London. Series A, Mathematical and Physical Sciences, Volume 219, Issue 1137, pp. 186-203

[3] Allouche, M, Static wall layers in the displacement of two visco-plastic fluids in a plane channel, J. Fluid Mech. (2000), vol. 424, pp. 243-277.

[4] Petitjeans, P, Miscible displacements in capillary tubes. Part 1. Experiments, J. fluid Mech. (1996), vol. 326, pp. 37-56

[5]Chen, C-Y, Miscible displacements in capillary tubes: Effect of a preexisting wall film, Physics of Fluids Volume 16, Number 3 March (2004)

[6] Lindner, A, Viscous fingering in non-Newtonian fluids, J. Fluid Mech. (2002), vol. 469, pp. 237-256

[7] De Souza Mendes, P, Liquid-Liquid Displacement Flows in an Annular Space Including Viscoplastic Effects, THE XV INTERNATIONAL CONGRESS ON RHEOLOGY: The Society of Rheology 80th Annual Meeting. AIP Conference Proceedings, Volume 1027, pp. 1381-1383 (2008).

[8] Zorin, Z, IMISCIBLE LIQUID-LIQUID DISPLACEMENT IN THIN QUARTZ CAPILLARIES, Advances in Co&d and Interface Science, 40 (1992) 85-108

[9] Chen, C,Y, Meiburg, E, Miscible displacements in capillary tubes. Part 2. Numerical simulations, J Fluid Mech. (1996), vol. 326, pp. 57-90

[10] Bakhtiyarov,, Fluid displacement in a horizontal tube, J. Non-Newtonian Fluid Mech., 65 (1996) l 15

[11]Yang, Z, Asymptotic solutions of miscible displacements in geometries of large aspect ratio, Physics of Fluids, Volume 9, Issue 2, February 1997, pp.286-298

[12] Vanapathy, S, H, Variable density and viscosity, miscible displacements in capillary tubes, European Journal of Mechanics B/Fluids 27 (2008) 268–289

[13] Chen, C,Y Miscible displacements in capillary tubes: Influence of Korteweg stresses and divergence effects, Physics of Fluids Volume 14, Number 7 July (2002)

[14] M, Regner Predicting the Displacement of Yoghurt by Water in a Pipe Using CFD, Chem. Eng. Technol. 2007, 30, No. 7, 844–853

[15] M, Regner CFD simulation and ERT visualization of the displacement of yoghurt by water on industrial scale, Journal of Food Engineering 80 (2007) 166–175

[16] Yang, Z, Asymptotic solutions of miscible displacements in geometries of large aspect ratio, Physics of Fluids, Volume 9, Issue 2, February 1997, pp.286-298

[17] Li,J, Direct simulation of unsteady axisymmetric Core annular flow with high viscosity ratio, J. Fluid Mech. (1999), vol. 391, pp. 123-149

[18] Valvekar, R, Numerical study of dispersed oil–water turbulent flow in horizontal tube, Journal of Petroleum Science and Engineering 65 (2009) 123–128

[19] Scoffoni, J, Interface instabilities during displacements of two miscible fluids in a vertical pipe, PHYSICS OF FLUIDS VOLUME 13, NUMBER 3 MARCH 2001

[20] Rakotomala, N, Miscible displacement between two parallel plates: BGK lattice gas simulations, J. Fluid Mech. (1997), vol. 338, pp. 277-297

[21] Reinalt, D, A, The penetration of a finger into a viscous fluid in a channel and tube, SIAM J. Sci. Stat. Comput. Vol. 6, No. 3, July 1985

[22] Rasmussen, H, K, Viscous flow with large fluid-fluid interface displacement, Int. J. Numer. Meth. Fluids 28: 859–881 (1998)

[23] Hydrodynamic simulation of the Rayleigh-Taylor instability. Government source: Shengtai Li, Hui Li [http://math.lanl.gov/Research/Highlights/amrmhd.shtml]

[24] Yih, C.S., Instability due to viscosity stratification J. Fluid Mech. (1967), vol. 27, part 2, pp. 337 352

[25] Instabilities of two immiscible fluids with different viscosities in a pipe J. Fluid Mech. (1984), vol. 131, pp. 309-317

[26] Kundu, P.K., Cohen, I.S., Fluid mechanics, 2010, fourth edition, ISBN: 978-0-12-381399-2

[27] Chhabra, R. P., Richardson, J.F., Non-Newtonian flow and applied rheology, 2008 Elsevier Second Edition, ISBN 978-0-7506-8532-0

[28] Pal, R. , Evaluation of theoretical viscosity models for concentrated emulsions at low capillary numbers, Chemical Engineering Journal vol 81 16-21

[29] Kiani, H, Rheological properties of Iranian yoghurt drink dough, International journal of dairy sciences vol 3 71 – 78

[30] Bayod, E., Micro structural and Rheological Properties of Concentrated Tomato Suspensions during Processing, 2008 doctorial thesis

[31] Yoon, W.B., McCarthy, K.L., Rheology of yoghurt during pipe flow as characterized by magnetic resonance imaging, 2002, Journal of Texture Studies 431–444

[32] White, F, Fluid Mechanics, 2006, 5th edition, ISBN 0072281928

[33] Rodi, W, Mulas, M. , Engineering turbulence modelling and experiments 6, 2005, ISBN 0 08 044544 6

[34] Yeoh, G, H, Tu, J, Computational Techniques for Multiphase Flows (2010), ISBN: 978-0-08-046733-7

[35] Fluent 6.3 user guide

[36] O. Ubbink Numerical predictions of two fluid systems with sharp interfaces, Doctorial thesis Department of Mechanical Engineering Imperial College of Science, Technology & Medicine, 1997

[37] CFD modeling of flow profiles and interfacial phenomena in two-phase flow in pipes
[38]Kim, S. S., Bhowmik, S. R., Effective Moisture Diffusivity of Plain Yogurt Undergoing Microwave Vacuum Drying, Journal of fluid engineering, vol 24, 137 – 148

[39] Hayaloglu, A.A et. al., Mathematical modeling of drying characteristics of strained yoghurt in a convective type tray-dryer, Journal of Food Engineering vol 78 109-117

[40] Koeltzsch, K, The height dependence of the turbulent Schmidt number within the boundary layer, Atmospheric Environment vol 34 1147-1151

[41] Tetra Pak data

[42] Potter, M.C, Mechanics of fluids, Third edition, Brooks/Cole, California , 2002 ISBN 978-0-5343-7996

[43] Hinze, J.O., 1975. Turbulence, Second edition, McGraw-Hill, New York.